Published online 20 December 2021

Nucleic Acids Research, 2022, Vol. 50, No. 2 ***1033–1051***
https://doi.org/10.1093/nar/gkab1231

Early rRNA processing is a stress-dependent regulatory event whose inhibition maintains nucleolar integrity

Witold Szaflarski[1,†], Marta Leśniczak-Staszak[1,†], Mateusz Sowiński[1], Sandeep Ojha[2,3], Anaïs Aulas[4], Dhwani Dave[5], Sulochan Malla[2,3], Paul Anderson[5,6], Pavel Ivanov[5,6] and Shawn M. Lyons[2,3,*]

[1]Department of Histology and Embryology, Poznan University of Medical Sciences, Poznań, Poland, [2]Department of Biochemistry, Boston University School of Medicine, Boston, MA, USA, [3]The Genome Science Institute, Boston University School of Medicine, Boston, MA, USA, [4]Predictive Oncology Laboratory, Cancer Research Center of Marseille (CRCM), Inserm U1068, CNRS UMR7258, Institut Paoli-Calmettes, Aix Marseille Université, Marseille, France, [5]Division of Rheumatology, Inflammation and Immunity, Brigham and Women's Hospital, Boston, MA, USA and [6]Department of Medicine, Harvard Medical School, Boston, MA, USA

Received August 24, 2020; Revised November 24, 2021; Editorial Decision November 26, 2021; Accepted December 02, 2021

ABSTRACT

The production of ribosomes is an energy-intensive process owing to the intricacy of these massive macromolecular machines. Each human ribosome contains 80 ribosomal proteins and four non-coding RNAs. Accurate assembly requires precise regulation of protein and RNA subunits. In response to stress, the integrated stress response (ISR) rapidly inhibits global translation. How rRNA is coordinately regulated with the rapid inhibition of ribosomal protein synthesis is not known. Here, we show that stress specifically inhibits the first step of rRNA processing. Unprocessed rRNA is stored within the nucleolus, and when stress resolves, it re-enters the ribosome biogenesis pathway. Retention of unprocessed rRNA within the nucleolus aids in the maintenance of this organelle. This response is independent of the ISR or inhibition of cellular translation but is independently regulated. Failure to coordinately control ribosomal protein translation and rRNA production results in nucleolar fragmentation. Our study unveils how the rapid translational shut-off in response to stress coordinates with rRNA synthesis production to maintain nucleolar integrity.

INTRODUCTION

Production of ribosomes is a major energetic and pro-growth task. Some estimates suggest that nearly 60% of the cell's energetic costs result from ribosome production (1). The expenditure of such a large percentage of energetic reserves is a result of the engagement of all three nuclear RNA polymerases (Pol I: 18S, 28S, 5.8S rRNA, Pol II: ribosomal protein mRNA, Pol III: 5S rRNA), coordination of ribosomal protein mRNA translation, chemical modification of rRNAs and assembly in the nucleolus. Compounding these energetic demands is the requirement for the accurate processing of the ∼13 000 nucleotide pre-rRNA (47S rRNA) into mature 18S, 5.8S, and 28S rRNAs. Again, estimates suggest that 60% of *de novo* RNA synthesis is rRNA. Maturation of the 47S rRNA requires multiple endonucleolytic and exonucleolytic processing events that generate a stereotyped series of pre-rRNA precursors (2). Much effort has gone into identifying the location of processing sites and identity of nucleases; however, there are specific processing sites where the responsible nuclease has yet to be determined (3). Further, these rRNAs are heavily chemically modified, making them second only to tRNAs in the percentage of modified nucleotides (4). The efficient assembly of ribosomes requires precise regulation of rRNA transcription, processing, modification, and delivery of newly synthesized ribosomal proteins from the cytoplasm to the nucleolus (5).

Transcription and many ribosome assembly steps take place in a specialized membrane-less organelle known as the nucleolus. The maintenance of the nucleolar structure is driven by a liquid-liquid phase separation (LLPS) (6). Two main factors responsible for this process are RNA and RNA-binding proteins that contain intrinsically disordered regions and low complexity sequences (IDR/LCS). Two major IDR-containing proteins in the nucleolus are fibrillarin (FBL) and nucleophosmin (NPM) (7–9). The concen-

*To whom correspondence should be addressed. Tel: +1 617 358 4490; Email: smlyons1@bu.edu
†The authors wish it to be known that, in their opinion, the first two authors should be regarded as joint First Authors.

tration of RNA processing and RNA modification enzymes in the nucleolus and other nuclear bodies increases processing and modification efficiency (10). Increases in nucleolar size or changes in nucleolar morphology are linked to increased growth demands owing to the necessity for new ribosomes in driving protein synthesis (11).

All cells encounter stress which activates cellular stress response pathways to promote cell survival (12,13). Diverse exogenous stresses, such as thermal stress, viral infection, oxidative stress, or nutrient deprivation, elicit an equally diverse array of cellular responses. A significant component of any pathway is to downregulate anabolic processes and redirect energetic reserves towards pro-survival functions. It has become clear that the nucleolus is an important stress-regulated organelle [reviewed in (14)]. This is unsurprising given the massive energetic cost of ribosome biogenesis and the pro-growth nature of protein synthesis. However, the effects on nucleolar structure or rRNA synthesis are not uniform. The normal nucleolar morphology is disrupted in response to transcriptional arrest caused by the DNA intercalating agent Actinomycin D (ActD) (15). This mode of transcriptional arrest results in the redistribution of many nucleolar proteins throughout the nucleoplasm and the formation of 'nucleolar caps' that contain nucleolar organizing regions (NORs) and distinct subsets of nuclear and nucleolar proteins (16,17). This phenotype is recapitulated in response to certain stresses, such as heat shock (18), serum starvation (19), nucleotide deprivation (20) and UV irradiation (21), in which the nucleolar structure is fragmented and disrupted (22). In these instances, a reduction in the nucleolar RNA content prevents LLPS formation or stability. Alternative stressors can result in different nucleolar morphologies known as 'nucleolar necklaces', in which late rRNA processing events become disconnected from rRNA transcription (23,24). Also of note is the formation of reversible amyloid structures in the nucleolus seeded by RNAs are transcribed by RNA polymerase II between rDNA genes in regions known as intergenic spacers (IGS) (25–27). These amyloids form in response to heat shock or acidosis and are thought to be cytoprotective.

The effects of cell stress are not constrained to alterations of the nucleolus. Adverse cellular conditions dramatically reduce the rates of protein synthesis [reviewed in (13)]. Generally, global modulation of these rates occurs via two non-mutually exclusive pathways: inactivation of mTOR signaling or activation of the 'integrated stress response (ISR).' mTOR is the primary regulator of cellular growth and promotes protein synthesis by keeping 4EBP proteins in an inactive state. Inactivating mTOR results in the dampening of translation initiation by preventing eukaryotic initiation factor 4F (eIF4F) formation (28,29). While mTOR inactivation affects the synthesis of many proteins, it has an outsized effect on the synthesis of ribosomal proteins (30). This is due to the added impact of a second mTOR target, LARP1, which specifically inhibits the translation of mRNAs encoding ribosomal proteins (31–33). Importantly, mTOR also controls rRNA synthesis by modulating basal transcription factors, UBF and TIF-IA/RRN3 (34–37). Thus, inactivation of mTOR leads to a co-regulated decrease in ribosomal protein synthesis and ribosomal RNA synthesis. This is important because cells must co-regulate ribosomal RNA production with the production of ribosomal proteins to maintain cellular homeostasis (38). Failure to do so results in nucleolar stress (39), which further compounds the initial cellular insult. Therefore, modulation of mTOR provides a self-contained mechanism to co-regulate both ribosomal protein synthesis and ribosomal RNA synthesis.

The ISR is the second major pathway that regulates global translation in response to stress (13). Four stress-responsive kinases (HRI, PERK, PKR and GCN2) sense different varieties of stress. Upon their activation, they phosphorylate the α-subunit of eukaryotic initiation factor 2 (eIF2α) to block translation initiation rapidly. Inhibition of translation by the ISR results in the formation of non-membranous RNA bodies called 'stress granules (SGs)' (40), which are storage sites for untranslated mRNPs. As with the inactivation of mTOR, activation of the ISR preferentially inhibits the translation of mRNAs that encode ribosomal proteins and targets these mRNAs to SGs (41). However, in contrast to mTOR-dependent regulation, little is known about how activation of the ISR, with subsequent repression of ribosomal protein synthesis, is co-regulated with rRNA synthesis. Further, the ISR is activated under acute stress conditions and rapidly inhibits translation (13). Thus, there is little leeway to regulate rRNA biosynthesis coordinately with the rapid shutoff of translation. We hypothesize that failure in such coordination results in a misallocation of energetic resources leading to further dysfunction.

Here, we show that stresses that induce eIF2α phosphorylation and SG formation also cause rRNA synthesis inhibition. Rather than directly inhibiting rRNA transcription by targeting the RNA polymerase I or associated basal transcription factors, leading to the disruption of the nucleolus, as has been shown for mTOR-dependent stress responses, we show that the first step in 47S rRNA processing is inhibited. As the rate of rRNA transcription is intrinsically tied to the efficiency of rRNA processing (42), failure to convert 47S rRNA into the next pre-RNA intermediate (45S rRNA) has the ultimate effect of repressing the rate of rDNA transcription. Therefore, rRNA production is 'paused' rather than being inhibited. The unprocessed pre-rRNA is stored within the nucleolus until stress has resolved, at which point it can re-enter the ribosome biogenesis pathway.

Moreover, this mechanism maintains nucleolar structure during stress as RNA contributes to the maintenance of this structure. Retention of unprocessed rRNA within the nucleolus during stress aids in nucleolar maintenance, such that when stress has passed, ribosome biogenesis machinery remains localized to the nucleolus. In contrast, direct inhibition of Pol I transcription compromises nucleolar integrity, thereby necessitating the nucleolus's reassembly after stress has passed. We show that despite being coordinated with eIF2α phosphorylation, an independent yet parallel event regulates stress-responsive modulation of rRNA processing. Finally, we show that failure to regulate rRNA production coordinately with translation results in nucleolar dysmorphology. Our data demonstrate that the first processing event in rRNA processing is regulated in a stress-dependent manner to conserve energetic reserves while balancing

ribosomal protein and rRNA synthesis and maintaining the nucleolar structure during stress.

MATERIALS AND METHODS

Antibodies

TIAR (Santa Cruz, sc-1749), NPM (Santa Cruz, sc-70392), FBL (Cell signaling Technology, 2639), RPA194 (Santa Cruz, sc-4669), eIF2α (Santa Cruz, sc-133132), phospho-eIF2α (AbCam, 131505), 4EBP (Cell Signaling Technology, 9454), non-phospho-4EBP (Cell Signaling Technology, 4923S), TIF-IA/RRN3 (Santa Cruz, 2c-390464), RPL7A (Cell Signaling Technology, 2415) Nol9 (Protein Tech Group, 16083-1-AP), UBF (Santa Cruz, sc-13125), eIF3B (Santa Cruz, sc-16377)

Cell culture and drug treatment

U2OS, HAP1 and HeLa cells were maintained in DMEM supplemented with 10% fetal bovine serum and Penicillin/Streptomycin. RPE1 cells were maintained in DMEM:F12 supplemented with 10% fetal bovine serum and Penicillin/Streptomycin. NIH3T3 were maintained in DMEM supplemented with 10% bovine calf serum and Penicillin/streptomycin in a humidified 37°C/5% CO_2 incubator. $NaAsO_2$ (Sigma), Lomustine (Selleckchem), H_2O_2 (Fisher), Actinomycin D (Arcos Organics), *N*-acetylcysteine (Sigma) were added for indicated times at indicated concentration. Where not noted, $NaAsO_2$ was treated at 200 μM.

Epifluorescence immunofluorescence

Cells were fixed and processed for fluorescence microscopy as described (43). Briefly, cells were grown on glass coverslips, stressed as indicated, and fixed with 4% paraformaldehyde in PBS for 15 min followed by 10 min post-fixation/permeabilization in −20°C methanol. Cells were blocked for 1 h in 5% horse serum/PBS. Primary and secondary antibody incubations were performed in blocking buffer for 1 h with rocking at room temperature. Secondary antibodies (Jackson Laboratories) were tagged with Cy2, Cy3 or Cy5. Following washes with PBS, cells were mounted in polyvinyl mounting media and viewed at room temperature using a Nikon Eclipse E800 microscope with a 40× Plan fluor (NA 0.75) or 100× Plan Apo objective lens (NA 1.4) and illuminated with a mercury lamp and standard filters for DAPI (UV-2A -360/40; 420/LP), Cy2 (FITC HQ 480/40; 535/50), Cy3 (Cy 3HQ 545/30; 610/75) and Cy5 (Cy 5 HQ 620/60; 700/75). Images were captured with SPOT Persuit digital camera (Diagnostic Instruments) with the manufacturer's software and compiled using Adobe Photoshop 2020.

Imaris 3D reconstruction and parametric analysis

For Imaris imaging, cells were treated in the same way as for epifluorescence immunofluorescence. The crude Z-stack images were collected using Olympus FV10i confocal laser scanning microscope. Then, images were processed with Imaris 7.4.2 (Bitplane, UK) for 3D reconstruction. The sizes of nuclei and nuclei were automatically calculated on the basis of Z-stacks composed of individual images. We then calculated the volume of all nucleoli in one nucleus in one cell. At least 100 cells from at least three independent experiments were taken for one analysis.

Metabolic labeling

For 5-ethynyl uridine labeling experiments, experiments were conducted using Click-iT RNA Alexa Fluor 488 Imaging Kit (ThermoFisher). Cells were prepared as for immunofluorescence, but 30 min prior to fixation, 5-EU was added to a final concentration of 1 mM. For [^{32}P]-metabolic labeling, cells were grown in a 6-well dish. Cells were starved for 1 h in phosphate-free DMEM containing 10% dialyzed FBS. Cells were then treated for 10 min with indicated compounds before adding 20 μCi of ^{32}P-*ortho*-phosphoric acid (Perkin Elmer). Cells were incubated for 1 h with media containing drugs and ^{32}P-*ortho*-phosphoric acid before replacing with DMEM containing 10% FBS with indicated drug treatment for an additional 1.5 h. RNA was harvested with Trizol reagent according to manufacturer's instructions and resuspended in 30 μl of RNA loading dye [58.3% formamide, 6.17% formaldehyde, 0.83× H–E buffer, 30 μg/ml Ethidium bromide, 40 μg/ml of bromophenol blue]. RNA was denatured at 85°C, and 10 μl were loaded onto a 1.2% Agarose gel made with 1× H–E buffer (20 mM HEPES, 1 mM EDTA [pH 7.8]) and 7% formaldehyde. Gels were run overnight in 1× H–E buffer at 55 V with recirculation and then dried and exposed to film.

L-Methyl-[^{3}H]-methionine pulse-chase

Cells were grown on a 60-mm plate. Cells were starved for 15 in pre-warmed methionine-free DMEM with dialyzed FBS at 37°C in a CO_2 humidified cell culture incubator. L-Methyl-[^{3}H]-methionine (Perkin-Elmer) was added to a final concentration of 50 μCi/ml. RNA was labeled for 30 min before replacing media with pre-warmed complete DMEM with 10% FBS supplemented with 0.3 mg/ml methionine. Cells were collected at indicated times and RNA was extracted using Trizol. Five micrograms of extracted RNA were resuspended in RNA loading dye and heated to 85°C for 10 min before placing on ice. Denatured RNA was electrophoresed as for [^{32}P]-metabolic labeling. The following day, the gel was subjected to mild alkaline treatment (10 min in 50 mM NaOH/10 mM NaCl), neutralization (10 min in 2.5× TBE) and equilibration in 2× SSC while rocking. RNA was transferred overnight by passive transfer to Hybond N$^+$ Nylon membrane using 20× SSC. The following day, nucleic acids were immobilized on the membrane by UV crosslinking. Membranes were exposed to Amersham Tritium phosphor screen for at least five days before detection using Typhoon phosphorimager.

Northern blotting

Cells were grown to ∼80% confluency and RNA was extracted with Trizol reagent (Invitrogen) according to manufacturer's instructions. 5 μg of RNA was prepared, electrophoresed and transferred to Hybond N$^+$ membrane

as with L-methyl-[^{3}H]-methionine pulse-chase experiments. Membranes were pre-hybridized in 10 ml of UltraHyb pre-hybridization/hybridization solution (Invitrogen) for 1 h at 60°C. Pre-hybridization solution was removed and 10 ml of fresh UltraHyb was added along with 15 μl of end-labeled northern probe. Probe was incubated for 1 h at 60°C and then overnight at 37°C. The following day, probes were washed twice with 2× SSC/0.1% SDS at 40°C and exposed to film. For stripping and re-probing, 50 ml of boiling 0.1× SSC/0.1% SDS was added to blots and allowed to come to room temperature twice.

Preparation of northern blotting probes

Synthetic DNA oligonucleotides were prepared by Integrated DNA Technologies and resuspended to a final concentration of 6 μM in dH_2O. For end-labeling, 1 μl of DNA was reacted with 2 μl of [^{32}P]-γ-ATP (3000 Ci/ml) (Perkin-Elmer), 1 μl of 10× T4 PNK buffer, 1 μl of T4 PNK (NEB) and 14 μl of dH_2O for 1 h. The reaction was brought to 100 μl with dH_2O and unincorporated nucleotides were removed by gel filtration through G-25 column (GE LifeSciences). The following oligonucleotide sequences were used for northern blotting: Human 5′ ETS (CGGAGGCCCAACCTCTCCGACGACAGGT CGCCAGAGGACAGCGTGTCAGC), Human ITS1 (GGCCTCGCCCTCCGGGCTCCGTTAATGAT), Human ITS2 (CTGCGAGGGAACCCCCAGCCGCGCA), Mouse 5′ETS (AAGCAGGAAGCGTGGCTCGGGG AGAGCTTCAGGCACCGCGACAGA), Mouse ITS1 (ACGCCGCCGCTCCTCCACAGTCTCCCGTTTAA TGATCC), Mouse ITS2 (ACCCACCGCAGCGGGTGA CGCGATTGATCG).

qRT-PCR

For qRT-PCR, cells were growing on 6-well plate. After treatment with the corresponding drug, total RNA was isolated using Universal RNA/miRNA Purification Kit (EURx, Poland). RNA was quantified using Nanodrop ND-1000 (ThermoScientific, USA). cDNA was obtained using LunaScript™ RT SuperMix Kit (New England Biolabs, USA) and qPCR reactions were performed using Luna® Universal qPCR Master Mix (New England Biolabs, USA) according to manufactural instructions. The qPCR reactions were done in CFX96 Touch Real-Time PCR Detection System (Bio-Rad, USA) and then analyzed in CFX Maestro Analysis Software (Bio-Rad, USA). The final graphs were prepared in GraphPad Prism 8. Primers for amplification spanned the A'/01 site, ensuring that only 47S and no other precursors were amplified. The sequences were: GTGCGTGTCAGGCGTTC and GGGA GAGGAGCAGACGAG.

RNA Fluorescence *In Situ* Hybridization

4 × 10^4 U2OS cells were seeded on coverslips and incubated overnight at 37°C with 5% CO_2 in DMEM supplemented media. Cells were stressed and then were fixed in 4% paraformaldehyde in PBS for 10 min and subsequently permeabilized in 98% cold methanol for 10 min. Cells were washed with 1× PBS and PerfectHyb™ Plus Hybridization Buffer (Sigma-Aldrich, H7033) was used to block samples (15 min at 62°C) and hybridize with Cy3 labeled FISH probes for 1 h at 62°C. FISH probes had the identical nucleotide sequence to those used for northern blotting. Then, samples were washed three times with 2× SSC and one time with PBS. Subsequently, cells were blocked with UltraPure™ BSA (0.5 mg/ml, Ambion, AM2616) prior to immunofluorescence. Finally, coverslips with cells were washed twice with PBS and mounted in polyvinyl mounting medium. Images were collected using Olympus FV10i laser scanned microscope and then parametrically analyzed using Imaris software.

FRAP

U2OS cells were transfected with plasmids containing tagged versions of RPL7A, Nol9 or NPM and selected with 0.8 mg/ml of geneticin. Stable cells were grown in 4-compartment 35 mm glass bottom dish (Greiner) until ∼80% confluency. Cells were treated with indicated drugs for 2 h before conducting FRAP on Zeiss as described previously (44). Acquired FRAP images were converted to parametric data with the use of ImageJ software and ImageJ macro programming language (45). Initially, image stacks were subjected to drift correction using Manual Drift Correction Plugin implemented into the ImageJ macro source code (Manual drift correction (Fiji), Benoit Lombardot). Transformed sequence image stacks were aligned with ROI of each bleached area for subsequent parametric data acquisition. The output parametric data from each ROI was grouped into 3 categories, encompassing: bleached, background and reference region. Results were exported to csv files and subsequently imported into R programming environment to facilitate calculations and plot generation (R Core Team (2019). R: A language and environment for statistical computing. R Foundation for Statistical Computing, Vienna, Austria (URL: https://www.R-project.org/). To eliminate noisy data Background Intensity Values (BG) were subtracted from Bleach Intensity Values (B) to obtain Bleach Corrected Values (B_corr) for each bleached region. Subsequently, Background Intensity Values were subtracted from Reference Intensity Values (Ref) to obtain Reference Corrected Values (Ref_corr). The final calculation was based on normalization of Bleach Corrected Values to Reference Corrected Values according to following equation: Normalized Bleach Corrected Values = Bleach Corrected Values/ Reference Corrected Values. Final data normalization, plots and total recovery summary tables were generated with the use of Frapplot package (Guanqiao Ding (2019). frapplot: Automatic Data Processing and Visualization for FRAP. R package version 0.1.3. URL: https://CRAN.R-project.org/package=frapplot).

CRISPR/Cas9 knockout of HRI

Oligonucleotides encoding gRNAs targeting the first exon of HRI were designed using CRISPR Design software from the Zhang lab (crispr.mit.edu). Oligonucleotides were annealed and cloned into pCas-Guide (Origene) according to manufacturer's protocol. gRNA targeting the first

exon of HRI contained the following sequence: GCCCTC GGCGGGAAAGTCGA. pCas-guide plasmids were co-transfected with pDonor-D09 (GeneCopoeia), which carries a puromycin resistance cassette, using Lipofectamine 2000 (Invitrogen). The following day, cells were selected with 1.5 μg/ml of puromycin. Selection was allowed to continue for 24 h to lessen the likelihood of genomic incorporation of pDonor-D09. Cells were screened based on their failure to form stress granules or phosphorylate eIF2α after exposure to $NaAsO_2$. Cells were cloned by limiting dilution. For genotyping, cells were resuspended at 10^8 cells/ml in digestion buffer (100 mM NaCl, 10 mM Tris [pH 8.0], 25 mM EDTA [pH 8.0], 0.5% SDS, 0.1 mg/ml proteinase K) and incubated overnight at 55°C. DNA was extracted with phenol/chloroform and precipitated with 2.5 M ammonium acetate and 2 volumes of 100% ethanol, washed with 70% ethanol and air-dried. DNA pellet was resuspended in TE containing 0.1% SDS and RNase A (1 μg/ml) and incubated at 37°C for 1 h. DNA was extracted with phenol/chloroform and precipitated as previously described. Resulting pellet was resuspended at a concentration of 100 ng/μl.

For genotyping, the first exon of HRI was amplified by PCR using primers located within the promoter and first intron (Forward: CTAGCTGCAGCATCGGAGT, Reverse: GAGGCAGACGTTCTTTTCAA) using AccuPrime G-C rich polymerase (Invitrogen). Amplicons were cloned into pGEM-T Easy vector (Promega) and sequenced.

RESULTS

We began our investigation of the connection between rRNA biosynthesis and stress response by analyzing the effect of stress on rRNA transcription using the 5-ethynyl uridine (5-EU) CLICK-IT assay. U2OS osteosarcoma cells were stressed for 90 min with $NaAsO_2$, the most widely used inducer of ISR, then 5-EU was added for an additional 30 min along with $NaAsO_2$ (Figure 1A). Alternatively, cells were left untreated or treated with ActD, a potent transcription inhibitor. Cells were fixed, permeabilized, and Alexa488 fluorophore was conjugated to the incorporated 5-EU to visualize nascent RNA. To mark the nucleolus, we used antibodies against NPM, a resident of the granular component (GC) subcomponent of the nucleolus. In control conditions, a high concentration of nascent RNA is present in the nucleolus, consistent with rRNA accounting for the vast majority of transcription (Figure 1Ba). We did not detect active transcription in the nucleolus after 90 min of ActD or $NaAsO_2$ treatment by this assay (Figure 1Bb–c). However, this presented a conundrum since nucleolar integrity was disrupted by ActD but not $NaAsO_2$. Therefore, we more directly interrogated rRNA by northern blotting. In humans, the primary ribosomal RNA transcript, termed the 47S rRNA, is polycistronic, containing the 18S, 28S and 5.8S rRNA. The mature rRNAs are flanked by 5′ and 3′ external transcribed spacers (5′ and 3′ETS) and separated by two internal transcribed spacers (ITS1 and ITS2). 47S rRNA is transcribed by RNA polymerase I and must be reiteratively processed by multiple enzymes to release the mature rRNAs (Figure 1C). The 5S rRNA is transcribed from other loci by RNA polymerase III. Using probes to different parts of the 47S transcript, we can analyze various rRNA processing intermediates. We began by examining the full 47S rRNA with a probe in the 5′ETS at the extreme 5′ end of the rRNA. Our previous work and others have shown that certain chemotherapeutic drugs are potent inducers of the ISR (46,47). A prevalent hypothesis has been that disrupting ribosome biogenesis would be a potent strategy in combating tumor progression. Therefore, we expanded our analysis to include the chemotherapeutic drug lomustine. Like $NaAsO_2$, lomustine induces phosphorylation of eIF2α, the hallmark of ISR induction, while ActD does not (Supplementary Figure S1A). However, both $NaAsO_2$ and Lomustine treatments resulted in an increase in 47S precursor rRNA and the formation of a faster migrating species (Figure 1D, ln 7, 8). The changes in 47S expression were independently confirmed by qRT-PCR (Figure 1E). The faster migrating species that has alternatively been termed the $30S^{+01}$ fragment or the 34S fragment is often seen when small subunit (SSU) processome is inhibited, e.g., under RNAi-mediated knockdown of certain RNA processing factors such as fibrillarin (48). This fragment results from a failure to process the first cleavage site, the A'/01 site (Figure 1C), and spurious processing at the 'site 2' site. Consistent with inhibition of the rRNA processing, as indicated by 34S generation, northern blotting for ITS1 and ITS2 revealed a profound decrease in downstream processing intermediates (e.g. 41S, 26S, 21S, 18S-E, and 12S) (Figure 1D and Supplementary Figure S1B – E). It is worth noting that northern blotting to ITS1 does not distinguish between the aberrant 34S product and canonical 30S precursors. Regardless, these data suggest that pre-rRNA processing is inhibited by preventing A'/01 processing, leading to an increase in 47S pre-rRNA and a decrease in downstream precursors. The proximal cause of acute stress by $NaAsO_2$ treatment is the generation of reactive oxygen species (ROS) resulting in oxidative stress (49). While long-term, chronic exposure to arsenic-containing proteins can have other detrimental biological effects, given our short treatment with $NaAsO_2$, we believe the effects are a result of ROS generation. To demonstrate that the proximate cause of rRNA stalling is in response to oxidative insult, we have co-treated cells with $NaAsO_2$ and *N*-acetyl cysteine (*N*-AC). *N*-AC raises the intracellular levels of glutathione ethyl ester (GSH) to protect against oxidative stress, preventing the AsO_2-induced ISR activation (47,50). Indeed, *N*-AC protects against stress-induced inhibition of rRNA processing (Figure 1F). Co-treatment with *N*-AC prevents 34S rRNA production and maintains the production of downstream precursors (26S, 21S, 18S-E, 12S).

The transcription factor p53 plays a significant role in the maintenance of the nucleolus (22,51). U2OS cells are a p53-positive cell line. To address the possibility that rRNA processing regulation was dependent upon p53, we performed the same experiments in HeLa cells, which are p53-null due to overexpression of the Human Papillomavirus E6 gene (52). We found that processing regulation was independent of p53 status as it occurs in both the p53-positive U2OS cells and the p53-deficient HeLa cells. We also wanted to address whether or not this regulation was specific to cancer cells, so we assayed non-cancerous human RPE-1 cells

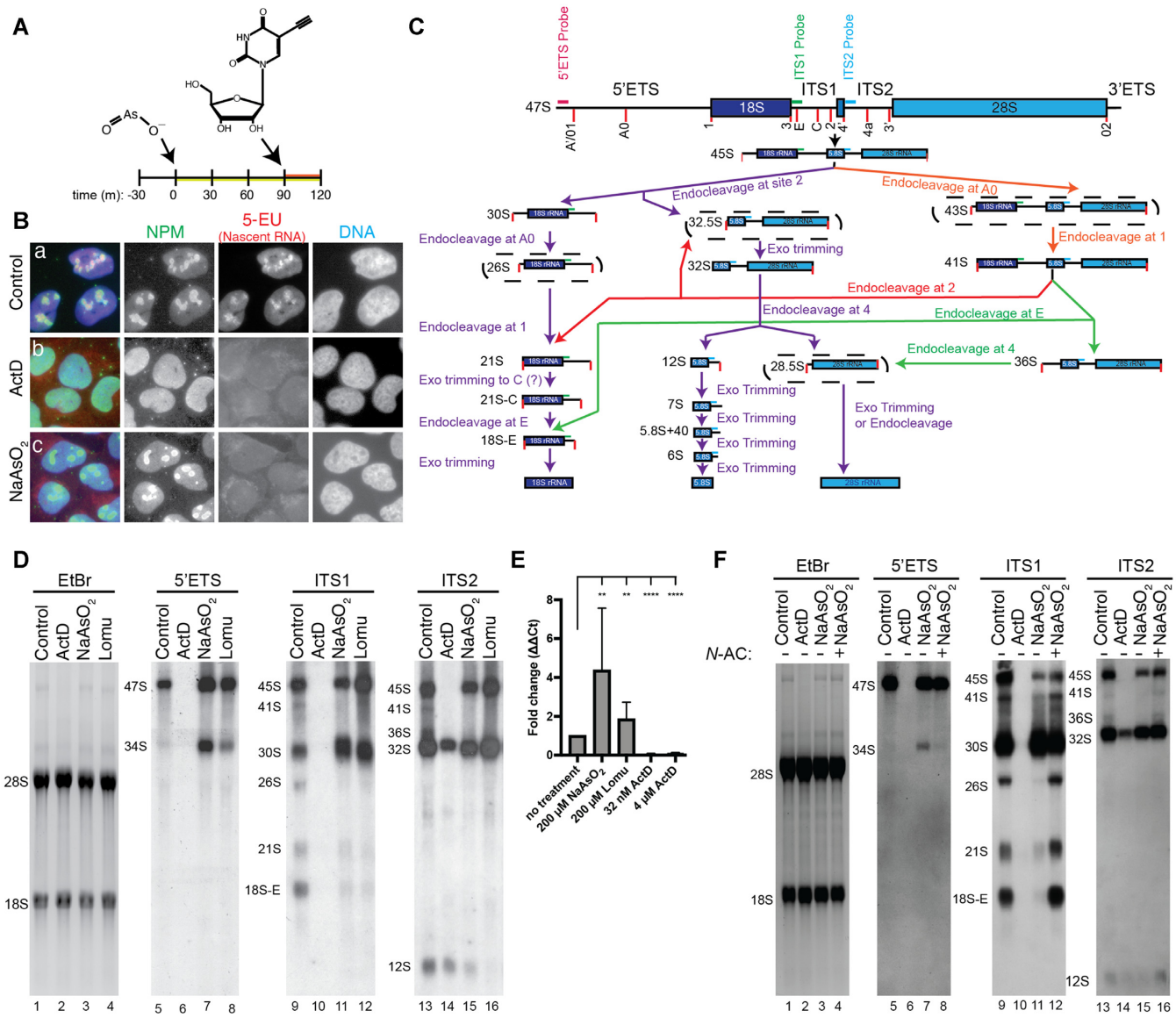

Figure 1. rRNA processing is inhibited in response to ISR-activating stress. (**A**) Schematic of 5-EU metabolic labeling experiment. Cells were stressed for 1.5 h and then 5-EU was added for 30 min to monitor transcriptional output. (**B**) Transcription in the nucleolus has been inhibited after 2 h of $NaAsO_2$-induced stress as indicated by loss of 5-EU signal in the nucleolus. (**C**) Schematic of the maturation pathway of human rRNAs. Approximate locations of northern blotting probes are noted in magenta, green and blue. (**D**) Northern blotting of cellular RNA after indicated treatments. 5 μg of RNA was resolved on 1.2% HEPES-EDTA agarose gel, transferred to nylon membrane and probed with indicated northern blotting probes. $NaAsO_2$ and lomustine result in accumulation of 47S pre-rRNA, the generation of the aberrant 34S product and the decrease in downstream precursors (18S-E, 21S, 26S, 41S, 12S). (**E**) qRT-PCR ($n = 3$) confirms increase in 47S pre-rRNA precursor after $NaAsO_2$ and Lomustine treatment and the decrease in 47S levels after ActD treatment. Data analyzed by Student's *t*-test (** $P < 0.01$, **** $P < 0.0001$). (**F**) Where indicated, cells were stressed with $NaAsO_2$ and co-treated with the ROS scavenger *N*-acetyl cysteine (*N*-AC, 5 mM). *N*-AC prevents inhibition of rRNA processing as indicated by the failure to generate the 34S precursor and the retention of downstream precursors.

that had been immortalized with hTERT. Again, we found the regulation as in the cancerous U2OS and HeLa cells (Supplementary Figure S1C). Finally, the A'/01 processing site is conserved in mice, so we wanted to assay if processing regulation was also conserved across evolution. Using NIH3T3 cells, we found the same increase in 47S rRNA, loss of downstream precursors, and generation of 34S pre-rRNA intermediate (Supplementary Figure S1D). Finally, we show that loss of downstream precursors and generation of the 34S fragment occurs in a dose-dependent and time-dependent manner (Supplementary Figure S1E). Therefore, stress-dependent regulation of rRNA processing is an evolutionarily conserved mode of stress response that occurs in response to various stresses in a p53-independent manner in both transformed and untransformed cells.

The rate and efficiency of RNA processing strongly affect the rate of transcription and vice-a-versa (42). That is, inhibition of rRNA processing can feedback to reduce rRNA transcription. The accumulation of 47S rRNA coupled with the loss of transcription after 90 min of stress sug-

gested that rRNA processing was inhibited, resulting in accumulation of the primary transcript (Figure 1D, E), which eventually results in cessation of RNA transcription (Figure 1A, B). Thus, we complemented our analysis of processing by [^{32}P]-metabolic labeling (Figure 2A–C). Here, cells were stressed, and [^{32}P]-*ortho*-phosphoric acid was added to monitor rRNA transcription and processing before chasing with cold, $NaAsO_2$-containing media for 2.5 h (Figure 2A). In control conditions, initial precursors (47S, 45S), intermediates (30, 32S) and mature rRNAs (28S, 18S) were all observed and matured over the 3.5-h time-course (Figure 2B, ln 15–21). However, after $NaAsO_2$ treatment, initial precursors were generated in agreement with northern blotting data. But these never matured to 18S and 28S rRNAs (Figure 2B, ln 22–28). We observed RNA species approximately the size of the 30S and 32S precursors that our northern blotting data, particularly our dose-response data (Supplementary Figure S1E), would suggest that it is the 34S fragment, not a canonical processing intermediate. However, this assay does not allow us to identify this fragment unambiguously. Regardless, these data confirm that rRNA maturation is inhibited by stress. Treatment with the transcriptional inhibitor Actinomycin D completely abolished new synthesis of rRNA (Figure 2C). We propose that inhibition of pre-rRNA processing serves to 'pause' ribosome biogenesis during a stress response. This occurs coordinately with inhibition of ribosomal protein biogenesis caused by eIF2α phosphorylation. However, for this 'pausing' to be an effective stress response strategy, the accumulated 47S rRNA should be utilized when stress has passed. Upon $NaAsO_2$ washout, eIF2α is rapidly dephosphorylated, and translation resumes (53). Cells were stressed with $NaAsO_2$ for 2 h, and then $NaAsO_2$-containing media was washed out and replaced with fresh media. After washout, cells were collected at indicated times, RNA was extracted and analyzed by northern blotting (Figure 2D). As before, $NaAsO_2$-induced oxidative stress results in generation of 34S precursor and a reduction of downstream precursors (Figure 2D, ln 2, 10, 18). However, within 90 min of $NaAsO_2$-washout, the levels of downstream precursor returned to control levels, indicating a rapid return to rRNA synthesis and processing (Figure 2D, ln 12, 21). More strikingly, during recovery, we noted new precursor rRNA species when probing for the 5′ETS. These represented 5′ cleavage products not seen during normal rRNA maturation. Under normal conditions, the first processing event (i.e. A'/01 cleavage) converts 47S to 45S pre-rRNA by removing the 5′ extreme ∼400 nts from the initial precursor (Figure 1C). Our data demonstrate that this event is blocked by stress allowing for the accumulation of precursors that retain this 5′ extension (47S and 34S). During recovery, processing resumes and results in a large influx of newly processed RNA at the A'/01 site, which results in an accumulation of the 1-A'/01 fragment at the same timepoints as we note a reduction in the 34S precursor (Figure 2D, ln 4–8). Additionally, we note the formation of a 1-A0 fragment. This fragment is generated from the processing of the 47S or 34S to the short-lived 26S or 43S intermediates (Figure 1C). Under normal conditions, these are generated from the 45S precursor, and thus this RNA would never be recognized by our 5′ETS probe. Typically, these 5′ cleavage products are degraded exonucleolytically (54). Whether the degradation system has become uncoupled from processing or the degradation machinery becomes overwhelmed because of a large influx of rRNA retaining the 1 – A'/01 fragment (Figure 1D, E) is unknown. However, the processing of these rRNAs, particularly the generation of the 1 – A0 fragment, suggests that stalled rRNAs are being processed at canonical sites upon return to homeostasis

To more directly assay if utilization of stalled rRNA occurs, we performed a pulse-chase experiment using L-methyl-[^{3}H]-methionine. In this assay, rRNA is labeled upon deposition of 2′*O*-methyl groups by snoRNPs. This approach allows for efficient chasing after labeling due to the rapid turnover of the cellular methionine pool. The timing of this experiment is critical for accurate interpretation (Figure 2E). Cells were stressed with $NaAsO_2$ concurrently with L-methyl-[^{3}H]-methionine for 30 min before chasing with excess cold methionine in the continued presence of $NaAsO_2$. Following 2 h of stress, $NaAsO_2$-containing media was replaced with normal media containing excess unlabeled methionine. Timepoints were taken at indicated points. Before recovery, L-methyl-[^{3}H]-methionine labeling was similar to [^{32}P]-metabolic labeling for both control and stressed cells (Figure 2F). However, labeled RNA was more efficiently chased from 47S/45S species to mature rRNAs in control conditions. When stressed cells were allowed to recover, precursor rRNAs that were labeled in the initial 30 min were efficiently chased to mature rRNAs. Therefore, during a stress response, rRNA processing stalls upon inhibition of processing at the A'/01 processing site, leading to the accumulation of 47S pre-rRNA. When stress resolves, this stored 47S pre-rRNA re-enters the biogenesis pathway leading to the production of mature rRNAs. It is important to note that these experiments also show that the rRNA generated during this time is methylated, an important step in ribosome biogenesis and functionality. However, we cannot rule out the possibility that rRNA generated during this process may be hyper- or hypomodified, which may contribute to heterogeneity seen in rRNA methylation (55).

The transcription and processing of rRNAs and the maturation of ribosomes occur in the nucleolus. Since this pathway is regulated in response to stress, we sought to investigate if stress triggers any changes to the nucleolus. While untransformed cells typically have 2–3 nucleoli, cancer cells often exhibit an increased number of nucleoli that are often of increased size, an observation linked with proliferative potential (11). Indeed, human osteosarcoma U2OS cells examined in this study have between 3 and 5 nucleoli on average as monitored by immunostaining against NPM (Figure 3Aa, B). Treatment of these cells with ActD significantly reduces the size or abolishes the nucleoli as monitored by NPM (Figure 3Ab, C) without affecting the nucleolar number of cells that retained nucleoli on a per-cell basis (Figure 3B). RNA and RNA-binding proteins (RBPs) are significant drivers of LLPS in non-membranous organelles (56). Thus, pharmaceutically induced transcription inhibition, such as by treatment with ActD, reduces RNA levels in the nucleolus, nucleolar structure is disrupted. However, as previously shown, this is not coincident with activation of the ISR (Supplementary Figure S1A), which is fur-

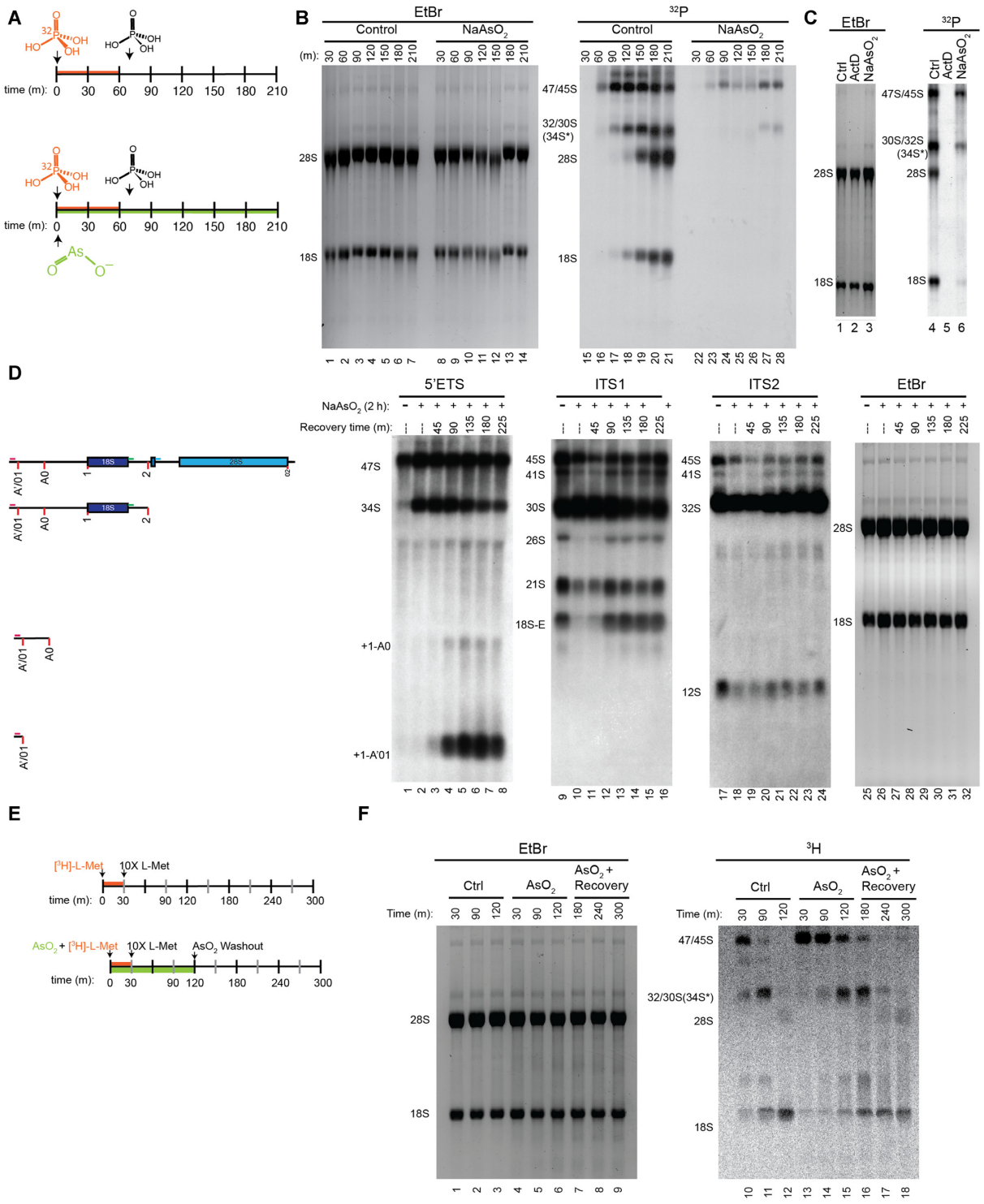

Figure 2. Stalled rRNA processing intermediates are utilized following a return to homeostasis. (**A**) Schematic of [^{32}P]-*ortho*-phosphoric acid labeling experiment. (**B**) $NaAsO_2$-treatment results in inhibition of rRNA processing. Large precursor rRNAs are generated, but the never mature into 18S and 28S rRNAs. *Upon $NaAsO_2$ treatment at late time-points, generation of a product of approximately the size of 30S and 32S is indistinguishable from 34S using this method. (**C**) End-point metabolic labeling with cells treated with $NaAsO_2$ or Actinomycin D (ActD). Whereas $NaAsO_2$ inhibits rRNA processing, ActD prevents rRNA transcription. (**D**) rRNA processing resumes rapidly during cell recovery. Cells were stressed for 2 h with $NaAsO_2$, at which point, $NaAsO_2$ was washed out and replaced with fresh media. Cells were allowed to recovery and timepoints were taken at indicated times followed by northern blotting. Downstream precursors return to control levels within 90 min of recovery. We also note the generation of 5′ cleavage products generated from 47S and 34S precursors. These non-canonical products are diagramed at left and noted as +1-A'/01 and +1-A0. (**E**) Schematic of L-*methyl*-[^{3}H]-methionine labeling experiment. Cells were stressed for 2 h, in which newly synthesized RNA was labeled for the first 30 min. After 2 h, $NaAsO_2$ was washed out and cells were allowed to recover over the indicated time course. (**F**) After $NaAsO_2$ washout, rRNA that was labeled during the initial phases of stress response re-entered the rRNA maturation pathway resulting in mature 18S and 28S rRNAs.

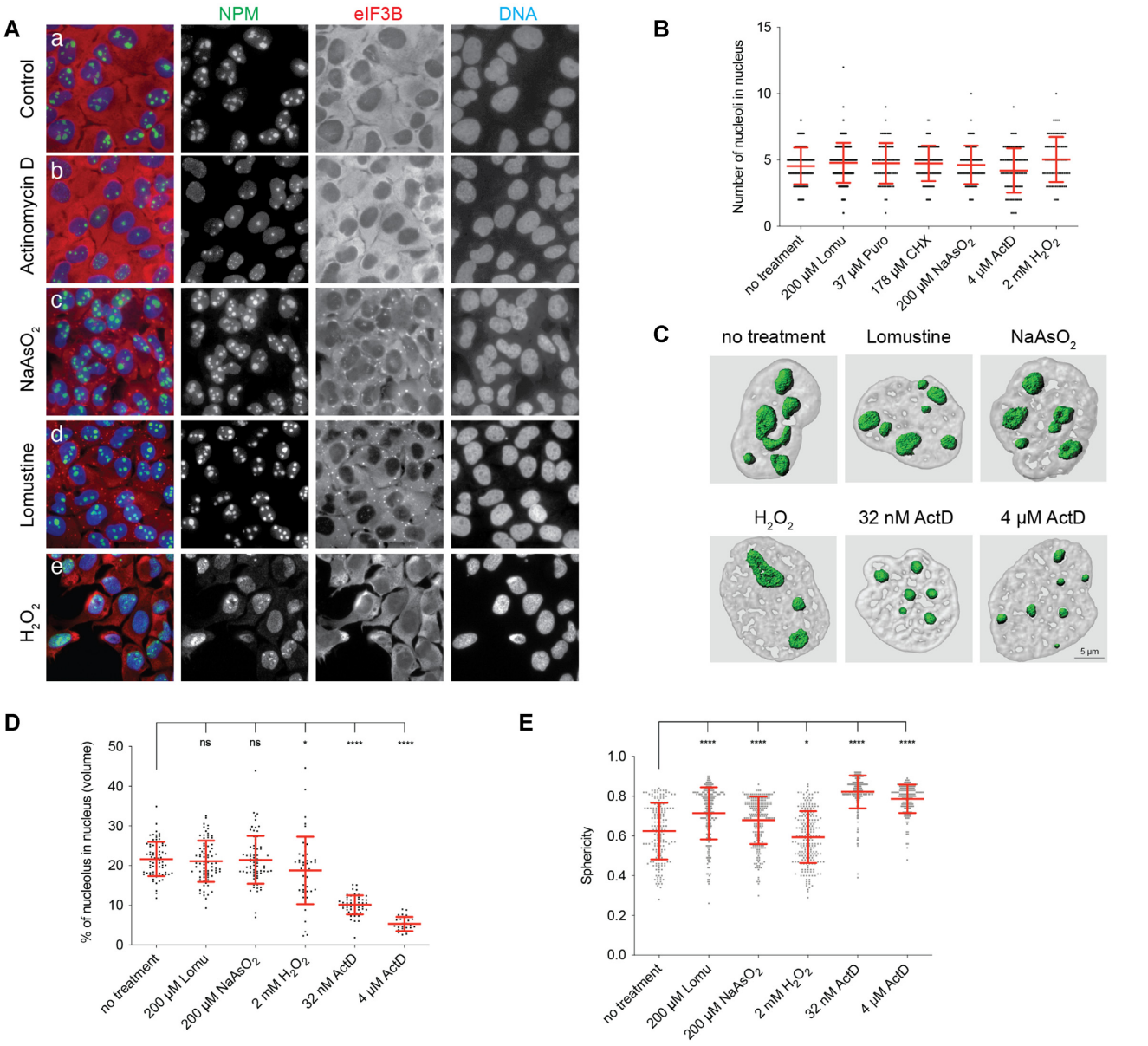

Figure 3. Nucleolar structure is maintained upon activation of the Integrated Stress Response. (**A**) Immunofluorescence of untreated U2OS osteosarcoma cells (**Aa**) or treated with Actinomycin D (**Ab**), $NaAsO_2$ (**Ac**), Lomustine H_2O_2 (**Ad**), or H_2O_2 (**Ae**). Nucleolar integrity was monitored by staining for nucleophosmin (NPM, green) and activation of the ISR was monitored by analysis of stress granule formation using eIF3B (red). (**B**) Nucleolar number is unaffected by stress response on a per cell basis. Cells were treated with indicated stresses and the number of retained nucleoli per nuclei were manually counted using NPM as a nucleolar marker. (**C**) Representative images of Imaris 3D reconstruction after indicated treatments. (**D**) Nucleolar volume is unaffected after ISR-activating stresses ($NaAsO_2$ and Lomustine), while volume is significantly decreased after mTOR-inactivating H_2O_2 treatment and ActD, which inhibits transcription. Data analyzed by Student's *t*-test (* $P < 0.05$, **** $P < 0.0001$). (**E**) Sphericity of nucleoli was determined following 3D reconstruction. ISR-activating stresses results in a more spherical nucleolar structure, while mTOR-inactivating H_2O_2 treatments results in a statistically significant decrease in sphericity Data analyzed by Student's *t*-test (* $P < 0.05$, **** $P < 0.0001$).

ther exemplified here by lack of stress granule formation as monitored by eIF3B localization (Figure 3Ab). Upon treatment with $NaAsO_2$ or lomustine, we induced the formation of stress granules and NPM-positive nucleoli remained (Figure 3Ac, d). NPM is but one marker of nucleoli that mass spectrometry analysis has determined contains over 270 proteins (57). These proteins are distributed throughout three subcompartments within the nucleoli: Granular Component (GC), Dense Fibrillar Component (DFC), and Fibrillar Center (FC). To ensure that NPM, a GC resident protein, was not unique in its nucleolar retention, we analyzed 11 additional nucleolar components by immunofluorescence representing members of each subcompartment and found no appreciable change in localization (Supplementary Figure S2A–H); however, future research will be needed to analyze more subtle changes in nucleolar substructures. As with regulation of rRNA processing, using HeLa cells, we also show that the persistence of the

nucleolus during stress is independent of p53 (Supplementary Figure S2I).

It is worth noting that these data seemingly contradict a previous report that showed that oxidative stress initiated by H_2O_2 inhibits rRNA synthesis via phosphorylation of TIF-IA, a basal polymerase I transcription factor (58). Thus, we sought to address this apparent discrepancy. In doing so, we repeated previously reported data by showing that H_2O_2-induced oxidative stress disrupts nucleolar architecture (Figure 3Ae, B–D). However, our previous data showed that H_2O_2 not only activates the ISR but also potently inhibits mTOR (59) as indicated by an increase in unphosphorylated 4EBP1 (Supplementary Figure S1A). Since mTOR is required for TIF-IA activation, the different targets of H_2O_2- and $NaAsO_2$-induced oxidative stress explain the apparent contradiction (35). We conclude that persistence of the nucleolus during stress is a feature of ISR-activating oxidative stress when mTOR is active, but not when it is inactive.

To further analyze nucleolar size and morphology, we employed Imaris imaging software to reconstruct 3D models of nucleolar structure under various cellular conditions to make parametrical analysis of the organelles and, consequently, more precise measurements (Figure 3C). This analysis revealed that upon initiating a stress response, there was no apparent change in nucleolar volume, in contrast to inhibition of transcription by ActD (Figure 3D). Immunofluorescence also suggested a shift in nucleolar morphology upon induction of a stress response, namely the adoption of more rounded morphology. We specifically quantified this by measuring sphericity as a ratio between the radius of an inscribing and circumscribing circle of the nucleoli. Thus, the more spherical the nucleoli, the closer the sphericity will be to 1, and the more oblong, the closer the shape will be to 0. Upon analysis, we showed a statistically significant increase in sphericity after $NaAsO_2$ and lomustine treatment, suggesting a change in the biophysical dynamics of this organelle (Figure 3E).

Since RNA is a contributing factor of nucleolar assembly via an RNA-driven liquid-liquid phase separation, we next sought to determine if this unprocessed rRNA was retained within the nucleolus, as would be suggested by the persistence of nucleoli and the utilization of stored pre-rRNA after stress (Figures 2 and 3). We performed RNA FISH in conjunction with immunofluorescence to analyze the localization of rRNA using Imaris 3D reconstruction. We utilized fluorescently labeled FISH probes that hybridized to the same locations as our northern blotting probes in the 5′ETS, ITS1 and ITS2. We used a low concentration of ActD (32 nM) to inhibit transcription to control for probe specificity. Note that at higher concentrations of ActD, the nucleolus is completely disrupted preventing parametric analysis (Figure 1B). Following stress, 47S rRNA was retained within the nucleolus, which aids in the preservation of nucleolar structure (Figure 4A & Supplementary Figure S3A). Consistent with northern blotting and qRT-PCR (Figure 1D and E) which demonstrated an increase in 47S/34S rRNA abundance, analysis with the 5′ETS probe demonstrates an increase in the volume of these precursors (Figure 4A and Supplementary Figure S3A). We also used FISH to assay other precursors using probes specific to ITS1 and ITS2, which similarly demonstrates that they remain localized to the nucleolus during stress (Figure 4B–C and Supplementary Figure S3B–C). Maintenance of this RNA in the nucleolus (Figure 4A–C), inhibition of processing (Figures 1 and 2), and increased nucleolar sphericity (Figure 3E) would suggest that the unprocessed RNA being stored in the nucleolus is affecting nucleolar dynamics during stress. We performed fluorescence recovery after photobleaching (FRAP) of nucleoli under stressed and unstressed conditions to assess this. Cell lines stably expressing mCherry-Nol9, an rRNA processing factor, GFP-RPL7A, a ribosomal protein, and mCherry-NPM were generated (Supplementary Figure S3D). We performed FRAP on control cells or cells treated with $NaAsO_2$ for 2 h (Figure 4D–G, Supplementary Figure S3D–F). Since the nucleolus is a highly active organelle, we were not surprised to find that fluorescence recovered nearly completely 45 s post-bleaching for each of the three tagged proteins, with NPM recovering after only 10–12 s post-bleach. However, $NaAsO_2$ treatment severely diminished nucleolar dynamics. We observed almost no recovery over the same timescale. Particularly striking was the change in the recovery of Nol9, an rRNA processing factor. These data confirm that in response to stress, the nucleoli serve as storage sites for unprocessed rRNA. The presence of this rRNA aids in the persistence of nucleoli.

We next sought to determine if regulation of rRNA processing in response to stress is a component of the ISR. To begin, we analyzed transcription 2 h post-stress using 5-EU as before (Figure 1A). The formation of stress granules is typically seen as a proxy for ISR activation (60). Thus, we treated cells with levels of $NaAsO_2$ below the level that fully induces SG formation (Figure 5A). At 75 μM $NaAsO_2$, approximately 50% of cells have visible SGs monitored by eIF3B staining. However, regardless of whether or not a cell has SGs, nucleolar transcription has ceased, suggesting that regulation of rRNA is independent of the ISR. To further explore whether activation of ISR is a requirement of stress-dependent rRNA regulation, we knocked out heme-regulated inhibitor kinase (HRI/EIF2AK1) using CRISPR/Cas9 (Supplementary Figure S4). HRI is one of four eIF2α-kinases (EIF2AKs) that respond to different stresses to inhibit protein synthesis in response to adverse conditions. We have previously shown that CRISPR/Cas9 knockout of HRI renders cells unresponsive to $NaAsO_2$ regarding eIF2α phosphorylation, translational repression, and SG formation (61). Therefore, we sought to determine whether rRNA processing and synthesis were still regulated in ΔHRI cell lines. SGs form in wild-type U2OS cells in response to $NaAsO_2$, while ΔHRI U2OS cells fail to form SGs (Figure 5B). However, 5-EU labeling of nascent RNA reveals transcriptional shutoff of nucleolar RNA synthesis 2 h post-stress in both WT and ΔHRI cells (Figure 5Bb and Bd).

To further explore the connection, or lack thereof, between the ISR and rRNA regulation, we utilized an additional cell line that we have previously demonstrated is deficient in ISR-activation derived from HAP1 cells (61). We used ΔHRI HAP1 cells that fail to phosphorylate eIF2α in response to oxidative stress and eIF2α(S51A) HAP1 cells in which HRI remains active, but eIF2α cannot be phospho-

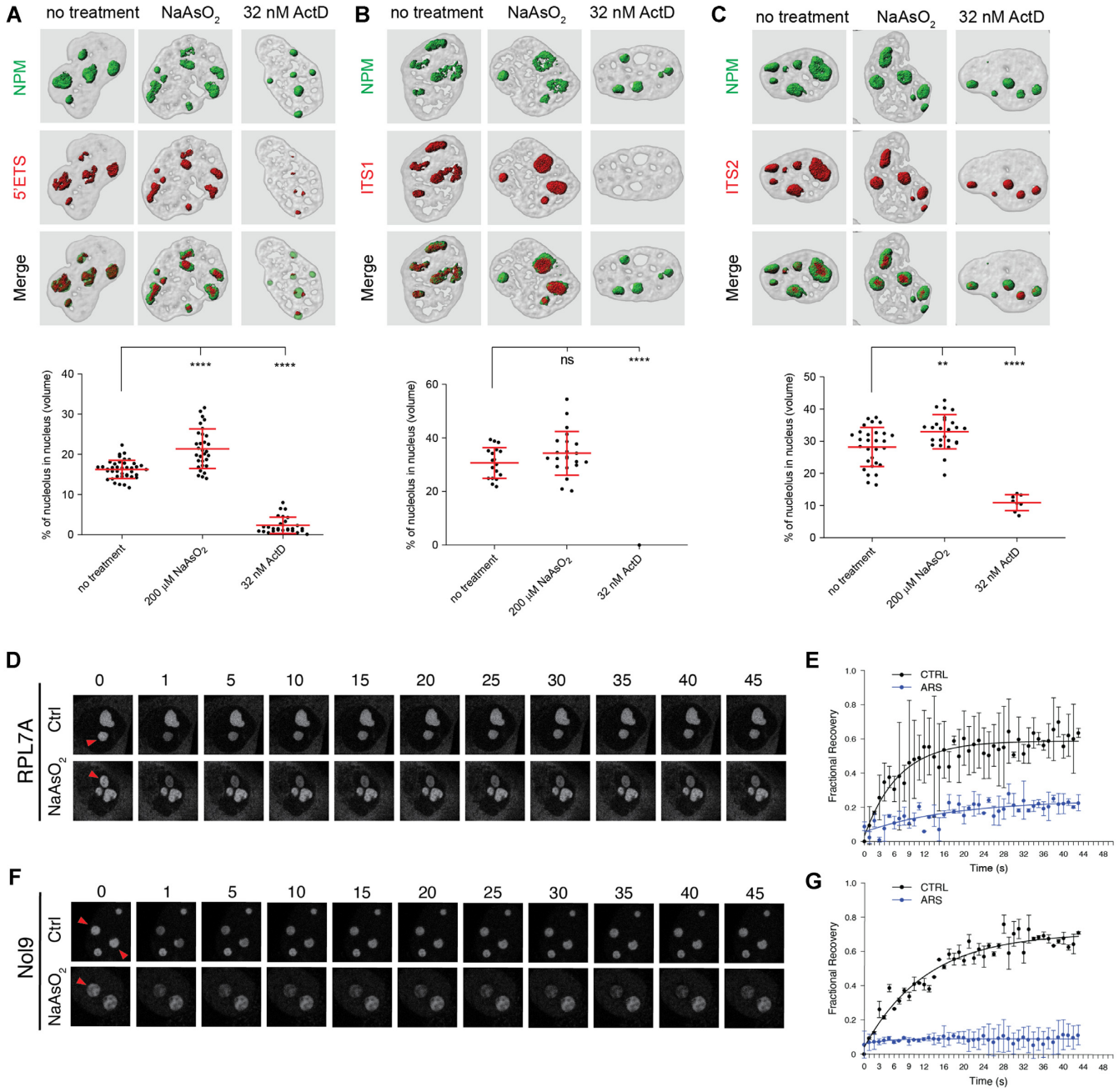

Figure 4. Unprocessed rRNA is stored in the nucleolus resulting in perturbed nucleolar dynamics. (A–C) 3D reconstructions of nucleoli after indicated treatment using NPM and FISH probes to (**A**) 5′ETS, (**B**) ITS1 and (**C**) ITS2. Parametric analysis of nucleolar volume based on FISH signal is represented below. Results demonstrate that unprocessed rRNA is retained within the nucleolus during a stress response. Data analyzed by Student's *t*-test (** $P < 0.01$, **** $P < 0.0001$). (D–G) Fluorescence recovery after photobleaching of RPL7A (**D–E**) or Nol9 (**F–G**) under basal and stressed conditions. Under nominal conditions, the bleached fluorescence signal rapidly recovers as expected by an active organelle. However, fluorescence recovery is severely perturbed during a stress response, consistent with the inhibition of rRNA processing. Red arrowheads denote the photobleached nucleoli.

rylated. Wild-Type, eIF2α(S51A) and ΔHRI HAP1 cells were stressed with $NaAsO_2$ as before. While translation is rapidly inhibited by $NaAsO_2$-induced oxidative stress in WT cells as monitored by ribopuromycilation, translation continues unabated in ΔHRI and eIF2α(S51A) cells resulting from a failure to effectively phosphorylate eIF2α (Figure 5C). However, when we analyzed rRNA precursors in these cells by northern blotting, we found that rRNA processing was blocked as indicated by the generation of the 34S precursor and loss of downstream precursors (Figure 5D). We conducted the same experiment in our newly generated ΔHRI U2OS cells and found similar results (Supplementary Figure S5A). These results suggest that inhibition of pre-rRNA processing occurs in a stress-dependent manner, independent of the ISR. Finally, we complemented our northern blotting by completing [^{32}P]-metabolic labeling

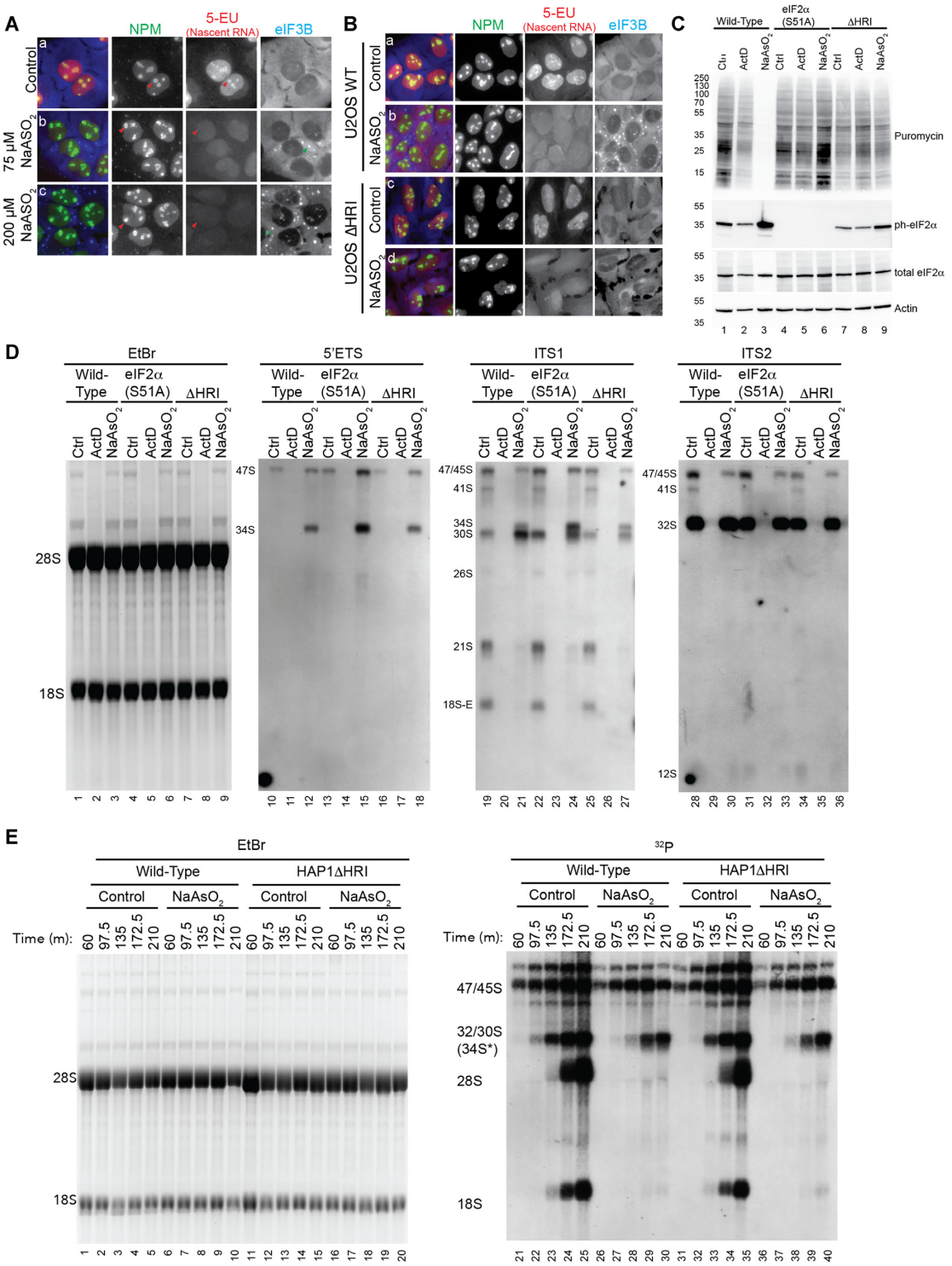

Figure 5. Regulation of rRNA processing in response to stress is parallel to, but not dependent upon, the ISR. (**A**) 5-EU metabolic labeling of U2OS cells was done as before with 0 μM (**Aa**), 75 μM (**Ab**) or 200 μM $NaAsO_2$ (**Ac**). Formation of stress granules, as monitored by eIF3B, was used as a proxy for activation of the ISR. rRNA transcription was impaired after 2 h of stress regardless of the formation of stress granules. Red arrowheads denote the nucleoli and green arrowheads denote stress granules. (**B**) 5-EU metabolic of **WT** (**Ba-b**) or U2OSΔHRI (**Bc-d**) cells untreated or treated with $NaAsO_2$. ΔHRI cells fail to form stress granules as translation is not regulated in these cells in response to stress. However, rRNA transcription is still inhibited 2 h post-stress induction. (**C**) WT, ΔHRI and eIF2α(S51A) HAP1 cells were stressed were treated as indicated and translational activity was assayed by ribopuromycilation. In response to $NaAsO_2$-induced oxidative stress, protein synthesis is inhibited in WT but not ΔHRI or eIF2α(S51A) cells as a result of failure to induce phosphorylation of eIF2α. (**D**) Northern blotting of rRNA in WT, ΔHRI and eIF2α(S51A) HAP1 cells. Despite the failure to active the integrated stress response, these cells continue to inhibit rRNA processing as indicated by generating the 34S fragment, diagnostic of processing inhibition (lns 12, 15 and 18) and leading to the reduction of downstream precursors (lns 21, 24, 27, 30, 33, 36). (**E**) [^{32}P]-metabolic labeling of WT and ΔHRI HAP1 cells demonstrate an inhibition in rRNA processing in response to cell stress despite a failure to inhibit translation.

experiments to monitor rRNA processing. We found that as in ΔHRI (Figure 5E) and eIF2α(S51A) (Supplementary Figure S5B) respond identically to WT cells. In both cases, 47S rRNA was generated, but this never matured to 28S or 18S rRNA after induction of a stress response. We also analyzed ΔHRI U2OS cells by [^{32}P]-metabolic labeling and found the same was true in this cell line (Supplementary Figure S5C). Therefore, we demonstrate that inhibition of early rRNA processing occurs concurrently but independently of the integrated stress response using two different, independently generated cell lines in different genetic backgrounds.

We have argued that stress-dependent regulation of rRNA processing maintains cellular homeostasis during stress by preventing excessive production of rRNA when ribosomal protein synthesis has been inhibited in the cytoplasm. Further, we argue that it functions to maintain the balance between ribosomal protein synthesis and rRNA synthesis, thereby preserving nucleolar integrity and protecting against nucleolar stress. To test this hypothesis and understand the consequences of disrupting this balance, we treated cells with puromycin (Puro) or cycloheximide (CHX). Both Puro and CHX are pharmacologic inhibitors of translation that do not activate the ISR or inactivate mTOR (Supplementary Figure S1A). They both directly target the translational machinery: Puro triggers premature translation termination while CHX stalls ribosome elongation. Therefore, treatment with these drugs would inhibit *de novo* ribosomal protein synthesis without directly targeting rRNA synthesis. Upon treatment of cells with CHX and Puro, we found similar results despite inhibiting translation through different mechanisms. We began by analyzing nucleolar dynamics by FRAP (Figure 6A–D). We argued that stress-induced decline in nucleolar dynamics served to maintain nucleolar structure after inhibiting ribosomal protein synthesis. However, upon translation inhibition by Puro or CHX, we found no significant change in nucleolar dynamics irrespective of the fact that new ribosomal proteins are not being delivered to the nucleolus (judging by either RPL7A (Figure 6A–B) or Nol9 (Figure 6C–D)). Next, we analyzed rRNA by northern blotting and found that 47S rRNA was still present without the production of the stress-dependent 34S fragment (Figure 6E). However, CHX and Puro treatment reduced the initial 47S rRNA precursor (Figure 6E, ln 9 and 10). Additionally, downstream precursors (e.g. 12S, 21S, 18S-E) are reduced upon treatment with Puro and CHX, consistent with the reduction of 47S. This is consistent with cells maintaining the balance between ribosomal protein and rRNA synthesis. However, pharmacological inhibition of ribosomal protein synthesis results in an inhibition of 47S synthesis but does not stall processing, resulting in a depletion of rRNA precursor species. Finally, we have argued that stress-dependent regulation of rRNA processing preserves nucleolar integrity when ribosomal protein synthesis has been inhibited. As CHX and Puro do not induce regulated inhibition of rRNA processing, we sought to determine the effect of continued rRNA production in the absence of ribosomal protein synthesis on nucleolar morphology by immunofluorescence (Figure 6F). As we found previously, the nucleolus was preserved after $NaAsO_2$-induced stress, with individual nucleoli adopting a more spherical morphology, concurrent with the formation of stress granules in the cytoplasm (Figure 6Fb). In contrast, neither CHX nor Puro induces SG formation, but there was a dramatic effect on nucleolar morphology (Figure 6Fc, d). Intact nucleoli adopted a 'ragged' morphology. However, more striking, was that the nucleoli in a subset of cells became fragmented, indicating a total loss of nucleolar integrity. The fact that there was no compensatory nucleolar response to the loss of ribosomal protein production likely contributes to the resultant nucleolar fragmentation. These results demonstrate the importance of stress-dependent regulation of rRNA processing in maintaining cellular homeostasis under stress.

DISCUSSION

Ribosomes are incredibly complex assemblies of RNA and protein subunits. Hundreds of assembly factors guide a single ribosome's biogenesis, which contains 79 individual proteins and four non-coding RNAs that can contain >200 chemical modifications (5). More than 70% of all transcription results from rRNA synthesis, and nearly 25% of all translation results from ribosomal protein synthesis, making ribosome biogenesis the most energy-intensive process in the cell (1). In addition to being generated on a large scale, ribosome biogenesis must also be precise, as malformed ribosomes are implicated in various disease states, including cancer and a diverse set of diseases known as 'ribosomopathies (62)'. A major task in guaranteeing the proper assembly of ribosomes is coordinating the expression of ribosomal RNA and ribosomal proteins. The biosynthesis of these individual components must be balanced to ensure homeostatic cell function (38,63,64).

Proper ribosome assembly requires remarkable synergy between diverse cellular machinery (Figure 7) [reviewed in (5)]. mRNAs encoding ribosomal proteins are transcribed by RNA polymerase II. The introns of these genes encode small nucleolar RNAs (snoRNAs) that guide rRNA's chemical modification. The mRNAs are capped, spliced, polyadenylated, and exported to the cytoplasm for translation. The intronic snoRNAs are further processed in the nucleus and assembled with proteinaceous factors to form snoRNPs. The ribosomal protein mRNAs harbor a specialized *cis*-element at their extreme 5′ end called a terminal oligopyrimidine (TOP) motif that aids in regulating their translation. Newly synthesized ribosomal proteins are imported into the nucleus and directed to the nucleolus. The nucleolus is established, in part, by the transcription of ribosomal RNAs. The 5S rRNA is transcribed by RNA polymerase III, and the 47S pre-rRNA is transcribed by RNA polymerase I. The nascent pre-rRNA is bound by snoRNPs, newly delivered ribosomal proteins, and other assembly factors. A subset of assembly factors includes RNA endonucleases that target specific pre-rRNA sites to release the mature rRNAs. Pre-ribosomes are exported to the cytoplasm, where final maturation occurs. At this point, assembled ribosomes are ready to take part in protein synthesis. The interdependency of such a complex system requires precise co-regulation of different components. Evolution has solved part of this problem by co-expressing many snoRNAs with ribosomal protein mRNAs; however, cells must

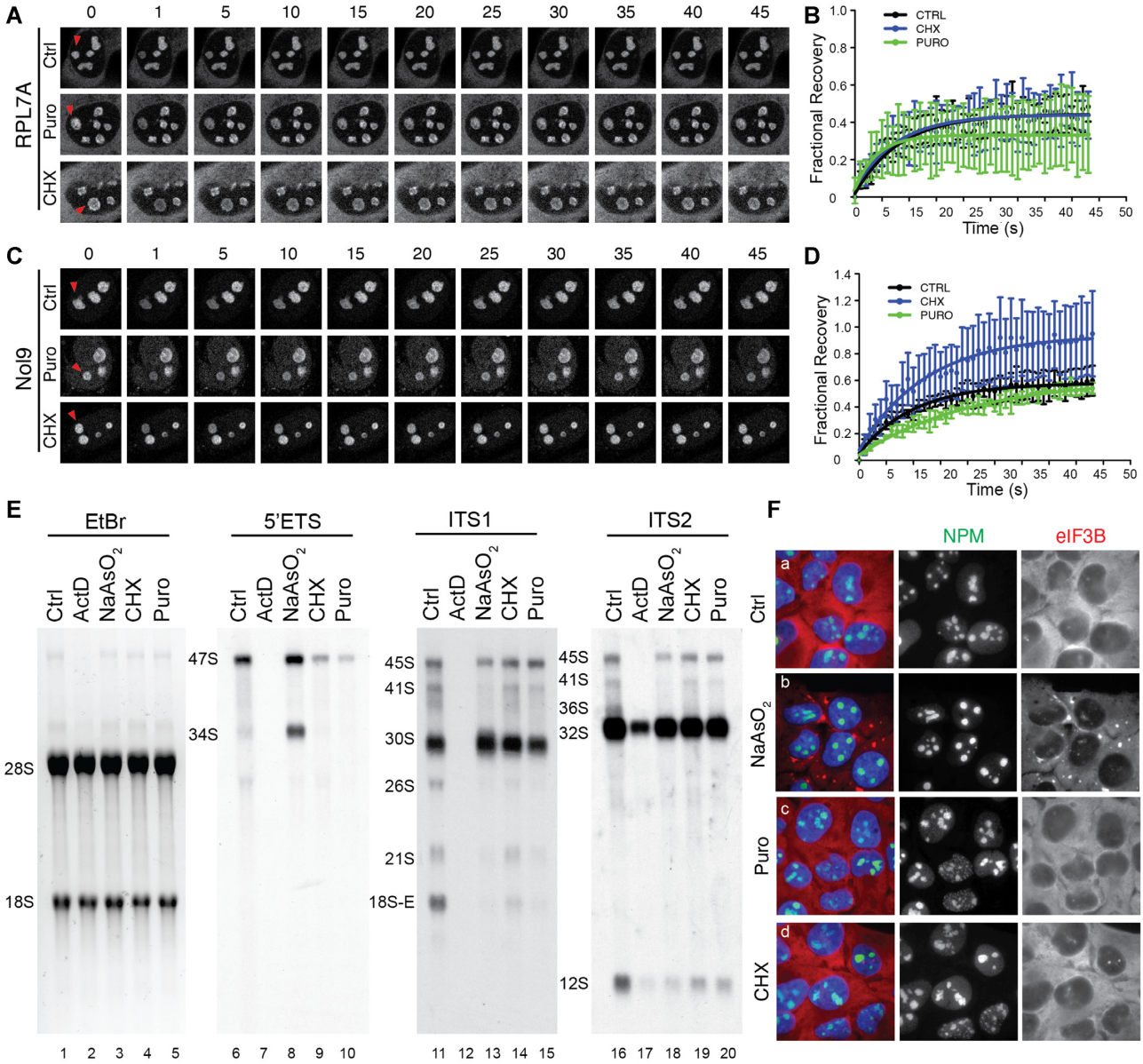

Figure 6. Failure to regulate rRNA processing with translation inhibition results in nucleolar fragmentation. (**A–D**) FRAP of U2OS cells stably expressing RPL7A (**A**, **B**) or Nol9 (**C**, **D**) untreated or treated with cycloheximide or puromycin to repress translation without inducing a stress response. Despite inhibition of translation, nucleolar dynamics remain unaltered indicating that previously identified alteration in nucleolar dynamics is not a result of translation inhibition. Red arrowheads denote photobleached nucleoli. (**E**) Northern blotting of rRNA after treatment with CHX and Puro demonstrates that 47S rRNA and 34S fragment do not accumulate. Instead, there is a reduction in 47S levels (ln 9 and 10) commensurate with the inhibition of ribosomal protein synthesis. (**F**) After indicated treatments, nucleoli of U2OS cells were analyzed by immunofluorescence by staining for NPM. Stress granule formation was monitored by eIF3B localization. As shown previously, $NaAsO_2$ results in stress granule formation and maintenance of nucleolar structure. However, translational inhibitors that do not trigger a stress response (CHX and Puro) result in fragmentation of nucleoli.

also maintain rRNA and ribosomal protein stoichiometry (38).

Under basal conditions, the regulatory machinery necessary for monitoring this process is complex. Stress exacerbates the need for strict regulatory controls over ribosome biogenesis. Cell stress activates multiple different pathways that aim at promoting cell survival until conditions return to normal. Curtailing pro-growth anabolic processes is a major goal of these pathways. As such, *de novo* protein synthesis, including synthesis of ribosomal proteins, is often rapidly inhibited. If the goal of promoting survival is to be realized by these pathways, they must also coordinately regulate the biogenesis of rRNA. The negative effects of failure to properly co-regulate assembly processes are revealed by pharmaceutical methods that inhibit protein or RNA synthesis.

Our data demonstrates that pharmaceutical inhibition of rRNA synthesis by ActD has little effect on global protein synthesis (Figure 5C). This is in line with previously reported data showing that ActD rapidly inhibits rRNA

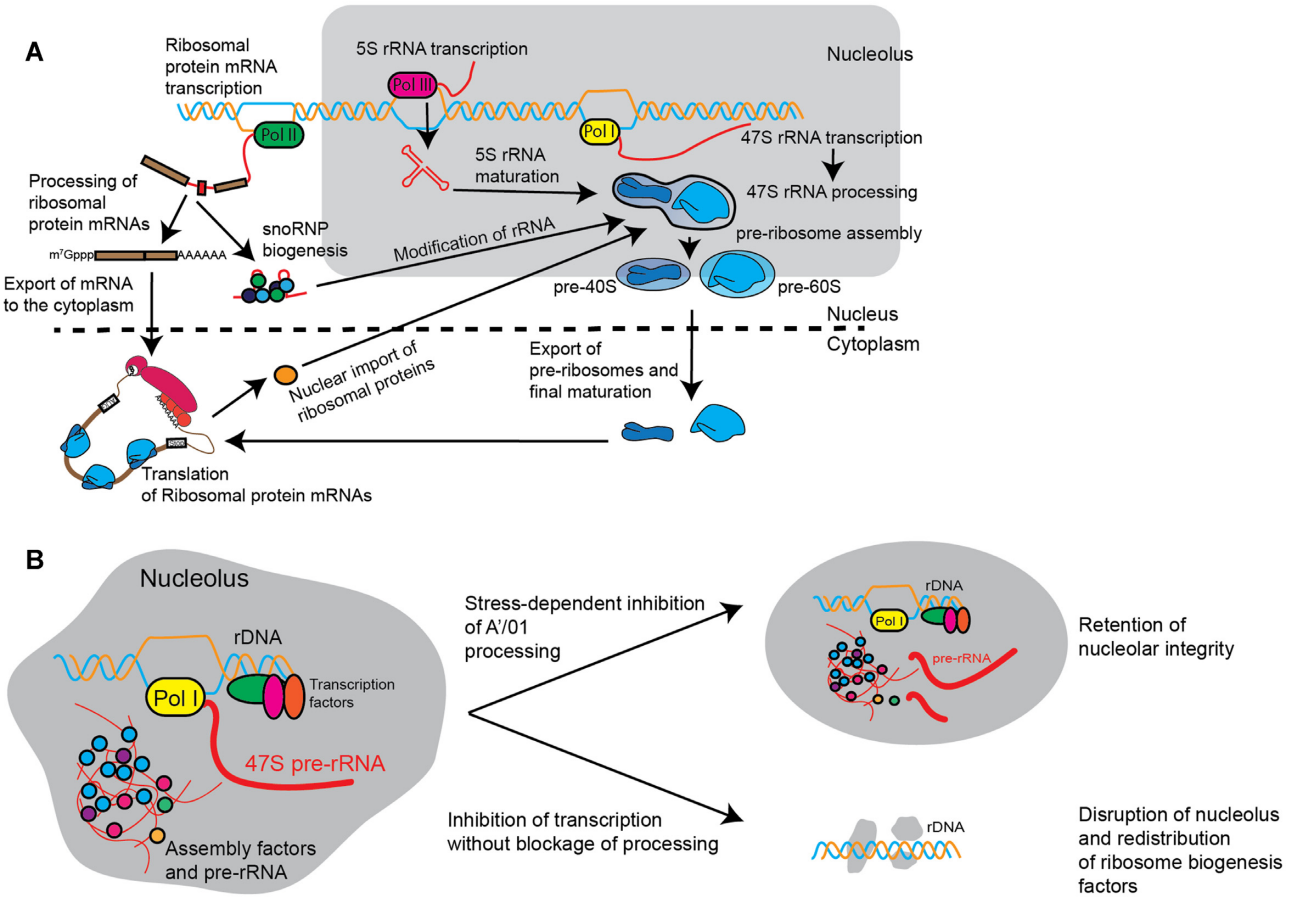

Figure 7. Overview of ribosome assembly and effect of inhibition of rRNA procession on nucleolar integrity. (**A**) Model of ribosome biogenesis demonstrating interconnected nature of assembly. Efficient assembly requires all three nuclear RNA polymerases, efficient pre-mRNA splicing and snoRNA biogenesis, transcription and processing of 5S and 47S rRNA. These pre-rRNAs must be chemically modified and complexed with newly synthesized ribosomal proteins. These events take place in the nucleolus, a phase-separated nuclear body. Sequestration to these nuclear bodies is thought to promote efficient processing and assembly. (**B**) Various stimuli can alter ribosome biogenesis. We demonstrate that inhibition of processing retains rRNA in the nucleolus in response to stress. As RNA and its association with RNA binding proteins is a major driver of phase separation, inhibition by this mechanism allows for the maintenance of nucleolar integrity. This is contrasted with methods that block transcription but allow for the continued maturation of rRNA. These conditions result in a depletion of rRNA in the nucleolus and a disruption of this nuclear body.

synthesis but does not affect the synthesis of ribosomal proteins (65,66). However, under these conditions, researchers found that newly synthesized ribosomal proteins are rapidly degraded. As the synthesis of ribosomal proteins can account for 25% of total protein synthesis (1), this represents a massive misallocation of energetic resources. If this occurs during stressed conditions, the outcomes could be catastrophic to the cell when cell viability is already challenged. We show that inhibition of protein synthesis without a regulated modulation of rRNA synthesis is equally detrimental. Pharmaceutical inhibition of protein synthesis reduces the abundance of rRNA precursors (Figure 6E). This has been corroborated by others that demonstrated a reduction in RNA polymerase I activity after CHX treatment (67,68). It should be noted that we cannot exclude the possibility that some pre-rRNA is degraded, as is the case for the obverse (i.e. protein degradation during inhibition of rRNA synthesis). However, the more striking outcome from this treatment is the effects on nucleolar morphology. Blocking protein synthesis in the cytoplasm results in perturbation of nucleolar morphology in the nucleus (Figure 6F). Nucleoli become dysmorphic with raggedy or torn edges. In a subset of cells, nucleoli undergo fragmentation and disruption, a hallmark of nucleolar stress, a condition resulting from an imbalance of individual components necessary for ribosome biogenesis and is associated with various disease states and cell death (14,22,36,39,51,69). Additionally, an siRNA screen revealed that knockdown of particular ribosomal proteins would similarly result in nucleolar dysmorphology, further highlighting the necessity to balance the production of individual ribosome components (70).

Given these concerns, when protein synthesis is blocked during a stress response, how does a cell regulate rRNA synthesis to prevent nucleolar stress? Two major pathways regulate global protein synthesis in response to stress: mTOR-dependent and ISR-dependent. mTOR is the catalytic component of two complexes, mTORC1 and mTORC2, regulating cell growth [Reviewed in (71)]. Under basal conditions, mTOR phosphorylates a variety of proteins to drive growth. In response to certain stressors (e.g., nutrient deprivation, hypoxia-induced oxidative stress), mTOR is inactivated, leading to the dephosphorylation of its target

proteins and a dampening of protein synthesis. mTOR integrates multiple aspects of ribosome biogenesis to allow for coordinative regulation of different components [Reviewed in (72)]. mTOR inactivation represses ribosomal protein synthesis through dephosphorylation of LARP1 (31) and represses the transcription of both 47S and 5S pre-rRNAs by modulating the activities of TIF-IA, UBF and Maf1 (35,73,74). This impressive signaling network allows for regulated control of each component of ribosomes.

It is less clear how or if rRNA synthesis is coordinately regulated upon activation of the ISR. While not universally true, the ISR is often thought of as reactive to acute stresses, such as UV irradiation, viral infection, and oxidative stress. A set of four stress-activated kinases (EIF2AKs) sense these different stresses (13). Upon their activation, they phosphorylate eIF2α to cause rapid cessation of protein synthesis, including ribosomal protein synthesis. Our current study demonstrates that ISR-activating stressors block rRNA synthesis by blocking the first step in rRNA maturation: cleavage at the A'/01 site of the 47S rRNA. $NaAsO_2$, the most commonly used ISR-inducing reagent, induces this response, as does the chemotherapeutic drug lomustine. Neither of these reagents trigger mTOR inactivation (Supplementary Figure S1A). Under this mode of regulation, unprocessed rRNA is stored within the nucleolus until a return to homeostasis, at which point the pre-rRNA re-enters the biogenesis pathway.

The efficiency of RNA transcription, regardless of the polymerase, is directly related to the efficiency of RNA processing. In RNA polymerase II-directed transcription, a wealth of data has been presented demonstrating the interconnected nature of RNA processing and transcription [Reviewed in (75)]. The demonstration that transcription and splicing are coordinated events led to the presupposition that the kinetics of these two events were interconnected (76). Later evidence demonstrated the rates of transcription and the efficiency of splicing and polyadenylation are connected (77–81). The crosstalk between mRNA transcription and pre-mRNA processing is largely coordinated by the carboxy-terminal domain (CTD) of RNA polymerase II, a domain lacking in RNA polymerase I (82). Yet, there remains an interplay between the rate of rRNA processing and rRNA transcription. In the current manuscript, we note that rRNA processing is inhibited, followed by an inhibition of rRNA transcription. The increase in the 47S precursor strongly suggests that inhibition of 47S processing precedes inhibition of rRNA synthesis. A lag in the inhibition of transcription leads to an increase in precursor levels (Figure 1D, E). Whether the blocking of processing is directly responsible for rRNA cessation of rRNA transcription or if later signaling events contribute to this inhibition is unclear. However, this mode of regulating is contrasted with those modes that directly block RNA polymerase I transcription (e.g. mTOR-dependent modulation of TIF-IA/UBF activity or ActD treatment). Loss of TIF-IA or phosphorylation-dependent inactivation of TIF-IA results in a loss of pre-rRNA and nucleolar disruption (58,83). Additionally, inhibition of mTOR by rapamycin perturbs nucleolar morphology by causing a redistribution of certain factors (e.g. NPM) (84).

We believe that a significant benefit of this mode of regulation is the preservation of nucleolar integrity. A major contributing factor to nucleolar structure is driven by a liquid-liquid phase separation (LLPS). FBL and NPM play important roles in establishing this structure the nucleolar LLPS (9,85). However, it has recently become clear one of the most critical drivers of LLPS is RNA [Reviewed in (86)]. Therefore, stresses or cellular conditions that deplete nucleolar pre-rRNA levels result in the dissolution of nucleolar structure (ActD, Figure 3). Nuclear bodies, including the nucleolus, are often formed around regions of high transcriptional output and serve to concentrate factors involved in RNA metabolism [Reviewed in (10)]. In addition to the nucleolus, this has been shown for other nuclear bodies, including the histone locus body (87) and Cajal bodies (88). Therefore, if a stress response were to result in the destruction of the nucleolus, this would only further hamper cell viability as the cell recovers from a cellular insult. Nucleolar components would be dispersed throughout the nucleoplasm and need to be relocalized to begin ribosome biogenesis. We propose that maintaining nucleolar structure may provide a fitness benefit as cells return homeostatic conditions. As all the proteins needed for is ensured upon the cessation of cellular insult without wasting an additional energy in reassembling this nuclear body.

It is worth pointing out that while mTOR-inhibition reduces transcription and pre-rRNA levels, there is also evidence that certain conditions block downstream processing events. The best evidence for this is derived from experiments in yeast, which lack the stress-responsive A'/01 processing site. In yeast, Tor1 signaling can promote a shift in ITS1 processing that results in the generation of an intermediate known as 23S precursor in response to heat shock and diamide-induced oxidative stress (89). Interestingly, this product is non-productive, as it does not reenter the biogenesis pathway upon return to homeostasis, a marked contrast to the mechanism described here in mammalian cells. In experiments studying the immediate effects on Tor1 inactivation in yeast, researchers found that RNA polymerase I remained associated with the rRNA promoter and was still found throughout the rRNA transcription unit (90). Within the first 15 min, the authors noted no reduction in the largest precursor, known as the 35S rRNA in yeast, but a striking inhibition of downstream precursors, suggesting that in response to Tor1 inhibition in yeast, the immediate effect is inhibition of processing, followed by an inhibition of transcription. Therefore, it is tempting to speculate that while the molecular players and processing sites have changed throughout evolution, there is a common evolutionary response.

Our data also suggests that conversion of the 47S to 45S rRNA is an obligatory step in rRNA biogenesis. When the pre-RNA matures to the 45S intermediate, there are multiple pathways through which the RNA intermediate can mature [reviewed in (2)]. However, our results demonstrate that, when stalled as the 47S rRNA, there is no alternative pathway that leads to mature 18S, 5.8S and 28S rRNAs. The fraction of 47S that gets processed to the 34S is not matured despite the fact that this represents the same RNA species as 30S rRNA except for the 5′ extension (i.e. 1-01 fragment). It is tempting to speculate that this region con-

tains an inhibitory sequence that prevents further processing. Alternatively, all rRNA processing enzymes could be simultaneously inhibited, but this would necessitate a hereto-fore unforeseen level of rRNA processing regulation. Another outstanding question is whether the 34S rRNA has any biological function. It is generated in a dose- and time-dependent manner during a stress response (Supplementary Figure S1E). This rRNA species has been observed upon the knockdown of rRNA processing components necessary for small subunit biogenesis (e.g. FBL) (48). Our FISH data demonstrates that this fragment is retained in the nucleolus, but whether it plays a functional or structural role there is unknown (Figure 4).

Importantly, the enzyme responsible for cleavage at the A'/01 site in the 5′ETS is unknown. This initial processing site is conserved in mice and humans (2), as is the stress-dependent regulation (Supplementary Figure S1). The sequence or functional equivalent is absent in yeast. Processing here and at the 02 site at the 3′ end of the pre-rRNA, convert the 47S rRNA to the 45S rRNA. The identity of this enzyme (or enzymes) and how its activity is regulated in response to stress are critical to gain a full understanding of the cellular stress response. We show that stress-dependent inhibition of rRNA processing occurs in parallel, but is not dependent upon, ISR activation (Figure 5). This suggests the existence of an alternative stress-responsive pathway found in the nucleus or nucleolus. However, further studies will demand the elucidation of this signaling pathway and how it regulates the activity of this unidentified endonuclease.

DATA AVAILABILITY

The authors declare that there are no primary datasets and computer codes associated with this study that are not contained within the manuscript.

SUPPLEMENTARY DATA

Supplementary Data are available at NAR Online.

ACKNOWLEDGEMENTS

We would like to thank Drs Barbara Sollner-Webb and Denis Lafontaine for helpful comments before submission of this manuscript and comments from Dr Michael Blower during revision.

Author contributions: S.M.L. conceived, designed and performed the analysis, interpreted results, and took the lead in writing the paper. W.S., M.L.-S, M.S., S.O., A.A., performed analysis, interpreted results and designed experiments. D.D. and S.M. performed analysis and aided in sample preparation. P.A. and P.I. gave critical feedback.

FUNDING

United States NIH [GM124458 to S.M.L., GM126150 to P.I., GM126901 to P.A.]; National Science Centre in Poland [UMO-2015/17/B/NZ7/03043 to W.S.]. Funding for open access charge: NIH.

Conflict of interest statement. None declared.

REFERENCES

1. Warner,J.R., Vilardell,J. and Sohn,J.H. (2001) Economics of ribosome biosynthesis. *Cold Spring Harb. Symp. Quant. Biol.*, **66**, 567–574.
2. Mullineux,S.T. and Lafontaine,D.L. (2012) Mapping the cleavage sites on mammalian pre-rRNAs: where do we stand? *Biochimie*, **94**, 1521–1532.
3. Henras,A.K., Plisson-Chastang,C., O'Donohue,M.F., Chakraborty,A. and Gleizes,P.E. (2015) An overview of pre-ribosomal RNA processing in eukaryotes. *Wiley Interdiscipl. Rev. RNA*, **6**, 225–242.
4. Taoka,M., Nobe,Y., Yamaki,Y., Sato,K., Ishikawa,H., Izumikawa,K., Yamauchi,Y., Hirota,K., Nakayama,H., Takahashi,N. *et al.* (2018) Landscape of the complete RNA chemical modifications in the human 80S ribosome. *Nucleic Acids Res.*, **46**, 9289–9298.
5. Bassler,J. and Hurt,E. (2019) Eukaryotic ribosome assembly. *Annu. Rev. Biochem.*, **88**, 281–306.
6. Brangwynne,C.P., Eckmann,C.R., Courson,D.S., Rybarska,A., Hoege,C., Gharakhani,J., Julicher,F. and Hyman,A.A. (2009) Germline P granules are liquid droplets that localize by controlled dissolution/condensation. *Science*, **324**, 1729–1732.
7. Feric,M., Vaidya,N., Harmon,T.S., Mitrea,D.M., Zhu,L., Richardson,T.M., Kriwacki,R.W., Pappu,R.V. and Brangwynne,C.P. (2016) Coexisting liquid phases underlie nucleolar subcompartments. *Cell*, **165**, 1686–1697.
8. Mitrea,D.M., Cika,J.A., Guy,C.S., Ban,D., Banerjee,P.R., Stanley,C.B., Nourse,A., Deniz,A.A. and Kriwacki,R.W. (2016) Nucleophosmin integrates within the nucleolus via multi-modal interactions with proteins disrplaying R-rich linear motifs and rRNA. *Elife*, **5**, e13571.
9. Yao,R.W., Xu,G., Wang,Y., Shan,L., Luan,P.F., Wang,Y., Wu,M., Yang,L.Z., Xing,Y.H., Yang,L. *et al.* (2019) Nascent Pre-rRNA sorting via phase separation drives the assembly of dense fibrillar components in the human nucleolus. *Mol. Cell*, **76**, 767–783.
10. Dundr,M. and Misteli,T. (2010) Biogenesis of nuclear bodies. *Cold Spring Harb. Perspect. Biol.*, **2**, a000711.
11. Montanaro,L., Trere,D. and Derenzini,M. (2008) Nucleolus, ribosomes, and cancer. *Am. J. Pathol.*, **173**, 301–310.
12. Spriggs,K.A., Bushell,M. and Willis,A.E. (2010) Translational regulation of gene expression during conditions of cell stress. *Mol. Cell*, **40**, 228–237.
13. Costa-Mattioli,M. and Walter,P. (2020) The integrated stress response: from mechanism to disease. *Science*, **368**, eaat5314.
14. Boulon,S., Westman,B.J., Hutten,S., Boisvert,F.M. and Lamond,A.I. (2010) The nucleolus under stress. *Mol. Cell*, **40**, 216–227.
15. Schoefl,G.I. (1964) The effect of actinomycin D on the fine structure of the nucleolus. *J. Ultrastruct. Res.*, **10**, 224–243.
16. Reynolds,R.C., Montgomery,P.O. and Hughes,B. (1964) Nucleolar "Caps" produced by Actinomycin D. *Cancer Res.*, **24**, 1269–1277.
17. Shav-Tal,Y., Blechman,J., Darzacq,X., Montagna,C., Dye,B.T., Patton,J.G., Singer,R.H. and Zipori,D. (2005) Dynamic sorting of nuclear components into distinct nucleolar caps during transcriptional inhibition. *Mol. Biol. Cell*, **16**, 2395–2413.
18. Liu,Y., Liang,S. and Tartakoff,A.M. (1996) Heat shock disassembles the nucleolus and inhibits nuclear protein import and poly(A)+ RNA export. *EMBO J.*, **15**, 6750–6757.
19. Chan,P.K., Aldrich,M. and Busch,H. (1985) Alterations in immunolocalization of the phosphoprotein B23 in HeLa cells during serum starvation. *Exp. Cell Res.*, **161**, 101–110.
20. Grummt,I. and Grummt,F. (1976) Control of nucleolar RNA synthesis by the intracellular pool sizes of ATP and GTP. *Cell*, **7**, 447–453.
21. Zatsepina,O.V., Voronkova,L.N., Sakharov,V.N. and Chentsov,Y.S. (1989) Ultrastructural changes in nucleoli and fibrillar centers under the effect of local ultraviolet microbeam irradiation of interphase culture cells. *Exp. Cell Res.*, **181**, 94–104.
22. Rubbi,C.P. and Milner,J. (2003) Disruption of the nucleolus mediates stabilization of p53 in response to DNA damage and other stresses. *EMBO J.*, **22**, 6068–6077.
23. Granick,D. (1975) Nucleolar necklaces in chick embryo fibroblast cells. I. Formation of necklaces by dichlororibobenzimidazole and other adenosine analogues that decrease RNA synthesis and degrade preribosomes. *J. Cell Biol.*, **65**, 398–417.

24. Louvet,E., Junera,H.R., Le Panse,S. and Hernandez-Verdun,D. (2005) Dynamics and compartmentation of the nucleolar processing machinery. *Exp. Cell Res.*, **304**, 457–470.
25. Audas,T.E., Audas,D.E., Jacob,M.D., Ho,J.J., Khacho,M., Wang,M., Perera,J.K., Gardiner,C., Bennett,C.A., Head,T. *et al.* (2016) Adaptation to stressors by systemic protein amyloidogenesis. *Dev. Cell*, **39**, 155–168.
26. Audas,T.E., Jacob,M.D. and Lee,S. (2012) Immobilization of proteins in the nucleolus by ribosomal intergenic spacer noncoding RNA. *Mol. Cell*, **45**, 147–157.
27. Lyons,S.M. and Anderson,P. (2016) RNA-Seeded functional amyloids balance growth and survival. *Dev. Cell*, **39**, 131–132.
28. Teleman,A.A., Chen,Y.W. and Cohen,S.M. (2005) 4E-BP functions as a metabolic brake used under stress conditions but not during normal growth. *Genes Dev.*, **19**, 1844–1848.
29. Gingras,A.C., Kennedy,S.G., O'Leary,M.A., Sonenberg,N. and Hay,N. (1998) 4E-BP1, a repressor of mRNA translation, is phosphorylated and inactivated by the Akt(PKB) signaling pathway. *Genes Dev.*, **12**, 502–513.
30. Thoreen,C.C., Chantranupong,L., Keys,H.R., Wang,T., Gray,N.S. and Sabatini,D.M. (2012) A unifying model for mTORC1-mediated regulation of mRNA translation. *Nature*, **485**, 109–113.
31. Fonseca,B.D., Zakaria,C., Jia,J.J., Graber,T.E., Svitkin,Y., Tahmasebi,S., Healy,D., Hoang,H.D., Jensen,J.M., Diao,I.T. *et al.* (2015) La-related protein 1 (LARP1) represses terminal oligopyrimidine (TOP) mRNA translation downstream of mTOR Complex 1 (mTORC1). *J. Biol. Chem.*, **290**, 15996–16020.
32. Smith,E.M., Benbahouche,N.E.H., Morris,K., Wilczynska,A., Gillen,S., Schmidt,T., Meijer,H.A., Jukes-Jones,R., Cain,K., Jones,C. *et al.* (2021) The mTOR regulated RNA-binding protein LARP1 requires PABPC1 for guided mRNA interaction. *Nucleic Acids Res.*, **49**, 458–478.
33. Hong,S., Freeberg,M.A., Han,T., Kamath,A., Yao,Y., Fukuda,T., Suzuki,T., Kim,J.K. and Inoki,K. (2017) LARP1 functions as a molecular switch for mTORC1-mediated translation of an essential class of mRNAs. *Elife*, **6**, e25237.
34. Hannan,K.M., Brandenburger,Y., Jenkins,A., Sharkey,K., Cavanaugh,A., Rothblum,L., Moss,T., Poortinga,G., McArthur,G.A., Pearson,R.B. *et al.* (2003) mTOR-dependent regulation of ribosomal gene transcription requires S6K1 and is mediated by phosphorylation of the carboxy-terminal activation domain of the nucleolar transcription factor UBF. *Mol. Cell. Biol.*, **23**, 8862–8877.
35. Mayer,C., Zhao,J., Yuan,X. and Grummt,I. (2004) mTOR-dependent activation of the transcription factor TIF-IA links rRNA synthesis to nutrient availability. *Genes Dev.*, **18**, 423–434.
36. Mayer,C. and Grummt,I. (2005) Cellular stress and nucleolar function. *Cell Cycle*, **4**, 1036–1038.
37. Mayer,C. and Grummt,I. (2006) Ribosome biogenesis and cell growth: mTOR coordinates transcription by all three classes of nuclear RNA polymerases. *Oncogene*, **25**, 6384–6391.
38. Gomez-Herreros,F., Rodriguez-Galan,O., Morillo-Huesca,M., Maya,D., Arista-Romero,M., de la Cruz,J., Chavez,S. and Munoz-Centeno,M.C. (2013) Balanced production of ribosome components is required for proper G1/S transition in Saccharomyces cerevisiae. *J. Biol. Chem.*, **288**, 31689–31700.
39. Yang,K., Yang,J. and Yi,J. (2018) Nucleolar Stress: hallmarks, sensing mechanism and diseases. *Cell Stress*, **2**, 125–140.
40. Panas,M.D., Ivanov,P. and Anderson,P. (2016) Mechanistic insights into mammalian stress granule dynamics. *J. Cell Biol.*, **215**, 313–323.
41. Damgaard,C.K. and Lykke-Andersen,J. (2011) Translational coregulation of 5′TOP mRNAs by TIA-1 and TIAR. *Genes Dev.*, **25**, 2057–2068.
42. Schneider,D.A., Michel,A., Sikes,M.L., Vu,L., Dodd,J.A., Salgia,S., Osheim,Y.N., Beyer,A.L. and Nomura,M. (2007) Transcription elongation by RNA polymerase I is linked to efficient rRNA processing and ribosome assembly. *Mol. Cell*, **26**, 217–229.
43. Lyons,S.M., Achorn,C., Kedersha,N.L., Anderson,P.J. and Ivanov,P. (2016) YB-1 regulates tiRNA-induced stress granule formation but not translational repression. *Nucleic. Acids. Res.*, **44**, 6949–6960.
44. Kedersha,N., Stoecklin,G., Ayodele,M., Yacono,P., Lykke-Andersen,J., Fitzler,M., Scheuner,D., Kaufman,R., Golan,D.E. and Anderson,P. (2005) Stress granules and processing bodies are dynamically liked sites of mRNP remodeling. *J. Cell Biol.*, **169**, 871–884.
45. Rueden,C.T., Schindelin,J., Hiner,M.C., DeZonia,B.E., Walter,A.E., Arena,E.T. and Eliceiri,K.W. (2017) ImageJ2: ImageJ for the next generation of scientific image data. *BMC Bioinformatics*, **18**, 529.
46. Catez,F., Dalla Venezia,N., Marcel,V., Zorbas,C., Lafontaine,D.L.J. and Diaz,J.J. (2019) Ribosome biogenesis: an emerging druggable pathway for cancer therapeutics. *Biochem. Pharmacol.*, **159**, 74–81.
47. Szaflarski,W., Fay,M.M., Kedersha,N., Zabel,M., Anderson,P. and Ivanov,P. (2016) Vinca alkaloid drugs promote stress-induced translational repression and stress granule formation. *Oncotarget*, **7**, 30307–30322.
48. Tafforeau,L., Zorbas,C., Langhendries,J.L., Mullineux,S.T., Stamatopoulou,V., Mullier,R., Wacheul,L. and Lafontaine,D.L. (2013) The complexity of human ribosome biogenesis revealed by systematic nucleolar screening of Pre-rRNA processing factors. *Mol. Cell*, **51**, 539–551.
49. Hu,Y., Li,J., Lou,B., Wu,R., Wang,G., Lu,C., Wang,H., Pi,J. and Xu,Y. (2020) The role of reactive oxygen species in arsenic toxicity. *Biomolecules*, **10**, 240.
50. Sun,S.Y. (2010) N-acetylcysteine, reactive oxygen species and beyond. *Cancer Biol. Ther.*, **9**, 109–110.
51. Woods,S.J., Hannan,K.M., Pearson,R.B. and Hannan,R.D. (2015) The nucleolus as a fundamental regulator of the p53 response and a new target for cancer therapy. *Biochim. Biophys. Acta*, **1849**, 821–829.
52. Liu,Y., Chen,J.J., Gao,Q., Dalal,S., Hong,Y., Mansur,C.P., Band,V. and Androphy,E.J. (1999) Multiple functions of human papillomavirus type 16 E6 contribute to the immortalization of mammary epithelial cells. *J. Virol.*, **73**, 7297–7307.
53. Novoa,I., Zhang,Y., Zeng,H., Jungreis,R., Harding,H.P. and Ron,D. (2003) Stress-induced gene expression requires programmed recovery from translational repression. *EMBO J.*, **22**, 1180–1187.
54. Kobylecki,K., Drazkowska,K., Kulinski,T.M., Dziembowski,A. and Tomecki,R. (2018) Elimination of 01/A'-A0 pre-rRNA processing by-product in human cells involves cooperative action of two nuclear exosome-associated nucleases: RRP6 and DIS3. *RNA*, **24**, 1677–1692.
55. Krogh,N., Jansson,M.D., Hafner,S.J., Tehler,D., Birkedal,U., Christensen-Dalsgaard,M., Lund,A.H. and Nielsen,H. (2016) Profiling of 2′-O-Me in human rRNA reveals a subset of fractionally modified positions and provides evidence for ribosome heterogeneity. *Nucleic Acids Res.*, **44**, 7884–7895.
56. Lin,Y., Protter,D.S., Rosen,M.K. and Parker,R. (2015) Formation and maturation of phase-separated liquid droplets by RNA-binding proteins. *Mol. Cell*, **60**, 208–219.
57. Andersen,J.S., Lyon,C.E., Fox,A.H., Leung,A.K., Lam,Y.W., Steen,H., Mann,M. and Lamond,A.I. (2002) Directed proteomic analysis of the human nucleolus. *Curr. Biol.*, **12**, 1–11.
58. Mayer,C., Bierhoff,H. and Grummt,I. (2005) The nucleolus as a stress sensor: JNK2 inactivates the transcription factor TIF-IA and down-regulates rRNA synthesis. *Genes Dev.*, **19**, 933–941.
59. Emara,M.M., Fujimura,K., Sciaranghella,D., Ivanova,V., Ivanov,P. and Anderson,P. (2012) Hydrogen peroxide induces stress granule formation independent of eIF2alpha phosphorylation. *Biochem. Biophys. Res. Commun.*, **423**, 763–769.
60. Kedersha,N., Ivanov,P. and Anderson,P. (2013) Stress granules and cell signaling: more than just a passing phase? *Trends Biochem. Sci.*, **38**, 494–506.
61. Aulas,A., Fay,M.M., Lyons,S.M., Achorn,C.A., Kedersha,N., Anderson,P. and Ivanov,P. (2017) Stress-specific differences in assembly and composition of stress granules and related foci. *J. Cell Sci.*, **130**, 927–937.
62. Mills,E.W. and Green,R. (2017) Ribosomopathies: there's strength in numbers. *Science*, **358**, eaan2755.
63. Donati,G., Bertoni,S., Brighenti,E., Vici,M., Trere,D., Volarevic,S., Montanaro,L. and Derenzini,M. (2011) The balance between rRNA and ribosomal protein synthesis up- and downregulates the tumour suppressor p53 in mammalian cells. *Oncogene*, **30**, 3274–3288.
64. Rudra,D., Mallick,J., Zhao,Y. and Warner,J.R. (2007) Potential interface between ribosomal protein production and pre-rRNA processing. *Mol. Cell. Biol.*, **27**, 4815–4824.
65. Warner,J.R. (1977) In the absence of ribosomal RNA synthesis, the ribosomal proteins of HeLa cells are synthesized normally and degraded rapidly. *J. Mol. Biol.*, **115**, 315–333.

66. Martinez-Ramon,A. (1979) Effects of actinomycin D on ribosomal RNA and protein synthesis as revealed by high resolution autoradiography. *Virchows Arch. B Cell Pathol. Incl. Mol. Pathol.*, **31**, 251–257.
67. Onishi,T., Matsui,T. and Muramatsu,M. (1977) Effect of cycloheximide on the nucleolar RNA synthesis in rat liver. Changes in RNA polymerase I and nucleolar template activity. *J. Biochem.*, **82**, 1109–1119.
68. Willems,M., Penman,M. and Penman,S. (1969) The regulation of RNA synthesis and processing in the nucleolus during inhibition of protein synthesis. *J. Cell Biol.*, **41**, 177–187.
69. James,A., Wang,Y., Raje,H., Rosby,R. and DiMario,P. (2014) Nucleolar stress with and without p53. *Nucleus*, **5**, 402–426.
70. Nicolas,E., Parisot,P., Pinto-Monteiro,C., de Walque,R., De Vleeschouwer,C. and Lafontaine,D.L. (2016) Involvement of human ribosomal proteins in nucleolar structure and p53-dependent nucleolar stress. *Nat. Commun.*, **7**, 11390.
71. Liu,G.Y. and Sabatini,D.M. (2020) mTOR at the nexus of nutrition, growth, ageing and disease. *Nat. Rev. Mol. Cell Biol.*, **21**, 183–203.
72. Iadevaia,V., Liu,R. and Proud,C.G. (2014) mTORC1 signaling controls multiple steps in ribosome biogenesis. *Semin. Cell Dev. Biol.*, **36**, 113–120.
73. Michels,A.A., Robitaille,A.M., Buczynski-Ruchonnet,D., Hodroj,W., Reina,J.H., Hall,M.N. and Hernandez,N. (2010) mTORC1 directly phosphorylates and regulates human MAF1. *Mol. Cell. Biol.*, **30**, 3749–3757.
74. Kantidakis,T., Ramsbottom,B.A., Birch,J.L., Dowding,S.N. and White,R.J. (2010) mTOR associates with TFIIIC, is found at tRNA and 5S rRNA genes, and targets their repressor Maf1. *Proc. Natl. Acad. Sci. U.S.A.*, **107**, 11823–11828.
75. Dujardin,G., Lafaille,C., Petrillo,E., Buggiano,V., Gomez Acuna,L.I., Fiszbein,A., Godoy Herz,M.A., Nieto Moreno,N., Munoz,M.J., Allo,M. *et al.* (2013) Transcriptional elongation and alternative splicing. *Biochim. Biophys. Acta*, **1829**, 134–140.
76. Jimenez-Garcia,L.F. and Spector,D.L. (1993) In vivo evidence that transcription and splicing are coordinated by a recruiting mechanism. *Cell*, **73**, 47–59.
77. McPheeters,D.S., Cremona,N., Sunder,S., Chen,H.M., Averbeck,N., Leatherwood,J. and Wise,J.A. (2009) A complex gene regulatory mechanism that operates at the nexus of multiple RNA processing decisions. *Nat. Struct. Mol. Biol.*, **16**, 255–264.
78. Nesic,D. and Maquat,L.E. (1994) Upstream introns influence the efficiency of final intron removal and RNA 3′-end formation. *Genes Dev.*, **8**, 363–375.
79. Niwa,M., Rose,S.D. and Berget,S.M. (1990) In vitro polyadenylation is stimulated by the presence of an upstream intron. *Genes Dev.*, **4**, 1552–1559.
80. de la Mata,M., Alonso,C.R., Kadener,S., Fededa,J.P., Blaustein,M., Pelisch,F., Cramer,P., Bentley,D. and Kornblihtt,A.R. (2003) A slow RNA polymerase II affects alternative splicing in vivo. *Mol. Cell*, **12**, 525–532.
81. Aslanzadeh,V., Huang,Y., Sanguinetti,G. and Beggs,J.D. (2018) Transcription rate strongly affects splicing fidelity and cotranscriptionality in budding yeast. *Genome Res.*, **28**, 203–213.
82. McCracken,S., Fong,N., Yankulov,K., Ballantyne,S., Pan,G., Greenblatt,J., Patterson,S.D., Wickens,M. and Bentley,D.L. (1997) The C-terminal domain of RNA polymerase II couples mRNA processing to transcription. *Nature*, **385**, 357–361.
83. Yuan,X., Zhou,Y., Casanova,E., Chai,M., Kiss,E., Grone,H.J., Schutz,G. and Grummt,I. (2005) Genetic inactivation of the transcription factor TIF-IA leads to nucleolar disruption, cell cycle arrest, and p53-mediated apoptosis. *Mol. Cell*, **19**, 77–87.
84. Iadevaia,V., Zhang,Z., Jan,E. and Proud,C.G. (2012) mTOR signaling regulates the processing of pre-rRNA in human cells. *Nucleic Acids Res.*, **40**, 2527–2539.
85. Mitrea,D.M., Cika,J.A., Stanley,C.B., Nourse,A., Onuchic,P.L., Banerjee,P.R., Phillips,A.H., Park,C.G., Deniz,A.A. and Kriwacki,R.W. (2018) Self-interaction of NPM1 modulates multiple mechanisms of liquid-liquid phase separation. *Nat. Commun.*, **9**, 842.
86. Van Treeck,B. and Parker,R. (2018) Emerging roles for intermolecular RNA-RNA interactions in RNP assemblies. *Cell*, **174**, 791–802.
87. Tatomer,D.C., Terzo,E., Curry,K.P., Salzler,H., Sabath,I., Zapotoczny,G., McKay,D.J., Dominski,Z., Marzluff,W.F. and Duronio,R.J. (2016) Concentrating pre-mRNA processing factors in the histone locus body facilitates efficient histone mRNA biogenesis. *J. Cell Biol.*, **213**, 557–570.
88. Xu,H., Pillai,R.S., Azzouz,T.N., Shpargel,K.B., Kambach,C., Hebert,M.D., Schumperli,D. and Matera,A.G. (2005) The C-terminal domain of coilin interacts with Sm proteins and U snRNPs. *Chromosoma*, **114**, 155–166.
89. Kos-Braun,I.C., Jung,I. and Kos,M. (2017) Tor1 and CK2 kinases control a switch between alternative ribosome biogenesis pathways in a growth-dependent manner. *PLoS Biol.*, **15**, e2000245.
90. Reiter,A., Steinbauer,R., Philippi,A., Gerber,J., Tschochner,H., Milkereit,P. and Griesenbeck,J. (2011) Reduction in ribosomal protein synthesis is sufficient to explain major effects on ribosome production after short-term TOR inactivation in Saccharomyces cerevisiae. *Mol. Cell. Biol.*, **31**, 803–817.